General Disclaimer

One or more of the Following Statements may affect this Document

- This document has been reproduced from the best copy furnished by the organizational source. It is being released in the interest of making available as much information as possible.

- This document may contain data, which exceeds the sheet parameters. It was furnished in this condition by the organizational source and is the best copy available.

- This document may contain tone-on-tone or color graphs, charts and/or pictures, which have been reproduced in black and white.

- This document is paginated as submitted by the original source.

- Portions of this document are not fully legible due to the historical nature of some of the material. However, it is the best reproduction available from the original submission.

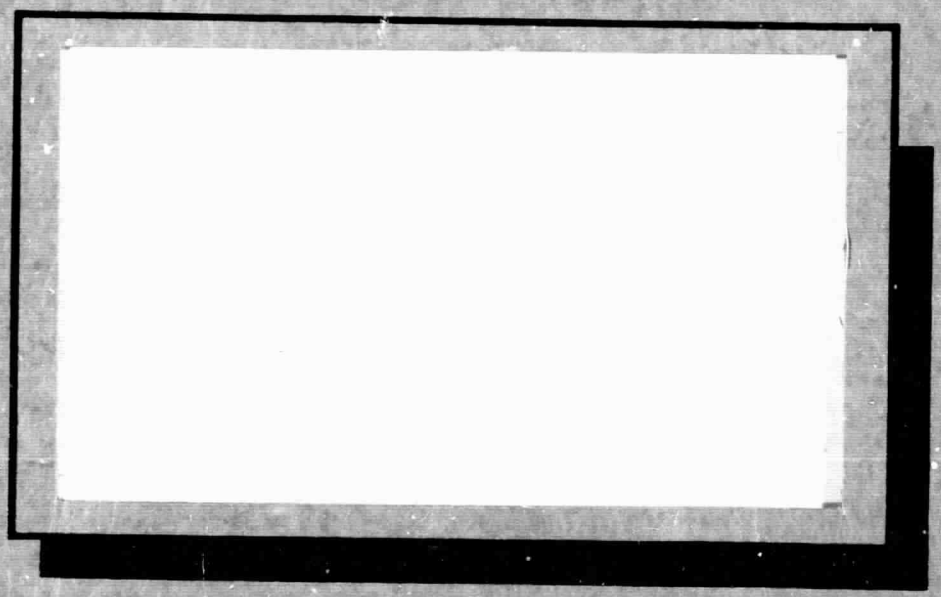

CENTER FOR SPACE RESEARCH
MASSACHUSETTS INSTITUTE OF TECHNOLOGY

Interim Report

Contract NAS 8-24585

A Preliminary Design Study for a Cosmic X-Ray Spectrometer

N. E.

Interim Report on Contract NAS 8-24585

A Preliminary Design Study for a Cosmic X-Ray Spectrometer

Massachusetts Institute of Technology

Principal Investigator: Prof. George W. Clark

Coinvestigator: Prof. Herbert W. Schnopper

Contract Termination Date: December 17, 1969

FOREWORD

This report describes the results of the work done on the design of a high resolution cosmic x-ray spectrometer under contract NAS 8-24585. It consists of a description of a "breadboard" spectrometer system and the results of the evaluation with this spectrometer of a number of different crystals, the results of theoretical studies made of the optical properties of this spectrometer used with an x-ray telescope, and a preliminary design and analysis of a number a detector systems that can be used with the spectrometer. Because work on the design and testing of the spectrometer and detector systems is continuing, this report is intended to be of the nature of an interim report rather than a final report.

This report represents the results to date of an effort undertaken by the staff of the Center for Space Research at the Massachusetts Institute of Technology for the Marshall Space Flight Center. The task is research and development leading towards the design of a cosmic x-ray spectrometer. The present increment of funding supported the effort from June 17, 1969 through December 17, 1969. Because this represented a gap of about six months between the expiration of the previous support period and the beginning of the present one, some key items could not be ordered on schedule. Several long lead time items were affected by this delay and, for example, the vacuum enclosure for the soft x-ray facility has only recently been delivered.

The highlights of the program are reviewed below according to items listed in the Program Plan of the Statement of Work. Progress toward the design of the spectrometer and ancillary equipment and their integration with the other experiments and subsystems of the grazing incidence telescope facility for an HEAO satellite has been reported in a series of meetings between the prospective investigators and NASA personnel. Our work has also been reported in a document[1] prepared by these investigators. In addition, two papers have been published[2,3] and a patent application[4] has been filed on work supported by this program.

1) Breadboard Model

A functioning breadboard model of the spectrometer has been constructed (Figs. 1 and 2). This version consists

of a point focus demountable x-ray tube (focal spot size of about .001 in. as measured by pin-hole pictures). The electron gun can be interchanged to provide ten times the intensity with a slightly larger focal spot size (about .004 in.). A wide range of target materials can be used in order to provide wavelength coverage over the range of interest. The exit window material is also replaceable. A separate vacuum system operates on the x-ray tube and the tube may be operated without the vacuum shroud. A 60 KV, 10 Ma stabilized power supply was assembled to power the tube. The spectrometer was designed to be very versatile so that many different modes of operation could be investigated in terms of the operating requirements of the orbiting version of this instrument. The radius of the Rowland circle is variable, and both the crystal and detector can be placed anywhere on or off the Rowland circle. The crystal angle can be set to any value and scanned in increments of 1.5 arcsec around that setting with a tangent arm and precision micrometer driven by a stepping motor. The crystal can be moved in or out along the line normal to its surface and inclined relative to the incident x-ray beam. Finally, as well as being moveable to the focus or any position off the focus, the detector can be scanned horizontally and vertically across the reflection pattern by a set of stepping motors. The mechanical motions and stepping motors are shown in Fig. 2a.

The original instrument was designed for a 20 inch focal diameter, but very good results are now obtained with 10 inches.

Film is used for establishing quickly the overall performance of a particular crystal under test. The reflection pattern can be investigated by a proportional counter with a pin-hole aperture (to simulate one cell in a microchannel array). The detector assembly can be rastered on an x-z table to scan an image region. The reflection pattern can also be investigated, and high resolution spectra obtained, by scanning the crystal around the Bragg angle in increments of 1.5 seconds of arc.

Since the vacuum shroud is not yet in operation (although it has been leak tested), results have been obtained using Cu Kα radiation in high orders of reflection to simulate the geometry which would obtain for low energy x-rays.

2), 3) Vacuum Shroud

In order fully to test the spectrometer at low energies it is necessary to evacuate the volume occupied by the instrument. A system to accomplish this was designed and constructed, but has not yet been made operational. The system was designed with enough flexibility to allow an additional program involving laboratory studies of x-ray phenomena of astrophysical interest to be conducted. In cooperation with the staff of the H. J. Van de Graaff Laboratory of the High Voltage Engineering Co., a program to measure precisely the spectra of x-rays from highly stripped atoms such as those in high temperature cosmic x-ray sources was begun. It was proposed that the MIT experiment be moved to the Van de Graaff installation, and our vacuum enclosure

has been designed with that purpose in view. As a consequence of the recent lack of funds for research support in the basic sciences, High Voltage Engineering Co. has recently closed the research laboratory. The MIT group is now looking for another functioning Van de Graaff group in order to continue the experiment.

4) Crystals

Mica has been the standard crystal used in the current evaluations. A diagram of the geometry of the spectrometer is shown in Fig. 3. Fig. 4 shows the reflection pattern of Cu $K\alpha_1$ and $K\alpha_2$ radiation from mica in 8th order for several crystal settings near the Bragg angle for $K\alpha_1$. Other crystals that were procured and tested were LiF (200), ADP, and KAP, all bent to a radius of 15" and ground for Johansson optics, and OHM, which was bent to a radius of 15" for Johann optics (section 5 contains a description of the different types of focusing optics). The reflection patterns of these crystals at several angles near the respective Bragg angles for Cu $K\alpha$ radiation are shown in Figs. 5, 6, 7, and 8. The ADP, KAP, and OHM were cracked in bending. In the cases of ADP and KAP this was due to the thickness required in order to be able to properly grind them for Johansson optics. Because of these cracks, the surface of the crystals deviated from the ideal surface, thus broadening the diffraction curve of the crystal as a whole and greatly decreasing its efficiency. The OHM developed cracks in bending because of its fragility, but techniques for bending it without cracking are being developed.

Furthermore, the OHM will be used for long wavelengths (25Å-64Å) where it has moderately low resolution (200-500), thereby not requiring precise bending. The width of the reflection patterns of the LiF, ADP, KAP, and OHM were approximately 12', 1.5°, 4°, and 1.5° respectively. It appears unlikely that ADP, KAP, and similar crystals could be bent and ground for Johansson optics with sufficient precision. The LiF did not develop cracks in bending, and the rocking curve for the crystal as a whole is not excessively broad (although it is still six times as broad as that for a perfectly bent crystal). The use of such techniques as heating the crystal and slowly bending it may well produce a crystal with a sufficiently narrow diffraction pattern. This and other techniques can also be used to bend similar crystals such as NaCl. Thus, LiF, NaCl, and possibly several other crystals should be investigated more closely. Also, the properties of ADP and KAP bent for Johann optics need to be investigated. When cut thin, these crystals do not develop cracks in bending and probably can be bent for Johann optics with sufficient precision. Small pieces of KAP have been cylindrically and spherically bent here to short radii without cracking.

In Figs. 5-8 a cone of radiation with a cone angle of approximately 10° was used. The radiation from an x-ray telescope, however, is in several annular rings each less than 1/2° wide. In the spectrometer this was approximated by an annulus 10° in outer diameter and 1° wide. Fig. 9 shows the

reflection pattern of this annulus from mica at several angular settings near the Bragg angle.

Table 1 gives the integrated reflectivities R_I, peak reflectivities R_p, and rocking curve widths at Cu Kα (1.54Å) for a number of crystals. The reflectivities and rocking curves of most crystals can be greatly changed by etching, polishing, grinding, abrasion, and thermal fracture. These techniques do not give consistently similar results when used on different crystal samples, and the results are a function of the wavelength range of interest, so that each crystal must be individually tailored to an approximate set of requirements through the use of one or a number of these techniques. The relative peak reflectivities and rocking curve widths in Å, Δλ, of several crystals with large 2d spacings are given in Table 2. The multilayer analyzers, Pb-Laurate, Pb-Stearate, and Pb-Lignoccerate show high reflectivities and are well worth investigating, but they are difficult to prepare well and are very unstable, especially in vacuum. As seen in this table, peak reflectivities and rocking curve widths are a function of wavelength. This is better shown in Figs. 9,10, and 11, which give the peak reflectivities and rocking curve widths in seconds of arc and electron volts for KAP from 2Å to 25Å. All of the numbers given in these figures and tables can be changed by appropriate selection and tailoring of the crystal. Also, the reflection efficiencies and rocking curve widths in Table 1 should not be extrapolated over a large wavelength range to establish the longer wavelength properties of these crystals,

Table 1

Integrated reflectivities, peak reflectivities, and rocking curve widths for various crystals at Cu Kα (1.5Å)[1]

Crystal	(Plane)	2d(Å)	Order	Surface	R_I	R_p	Rocking Curve Full Width at Half Maximum (sec.)
LiF	(200)	4.026	1	cleaved	8.8×10^{-5}	7.5%	185
LiF	(200)			etched	8.8×10^{-5}	7.5%	185
LiF	(200)			polished	2×10^{-4}	23%	100
LiF	(200)			ground	3.8×10^{-4}	25%	150
LiF	(200)			abraded	6×10^{-4}	20%	500
LiF	(200)			abraded	4.4×10^{-4}	27%	300
LiF	(220)		1	ground	1.4×10^{-4}	6%	330
LiF	(220)			etched	1.4×10^{-4}	6.6%	240
LiF	(220)			polished	1.5×10^{-4}	9.1%	160
EDDT	(010)		1	polished	1.2×10^{-4}	31.5%	40
EDDT	(010)			ground	8.6×10^{-5}	32%	29
PET	(001)	8.742	1	cleaved and polished	1.1×10^{-4}	27%	55
SHA	(110)	13.98	2	as grown	1.0×10^{-4}		45
RAP	(001)	26.12	5	cleaved	8×10^{-5}		13
KAP	(001)	26.63	7	cleaved	4.1×10^{-5}		10

[1] In part from I. W. Ruderman and B. Michelman, Present Status of X-Ray Analyzer Crystals, Isomet Corp. report.

Table 2

Relative peak reflectivities and crystal resolutions for various crystals[1]

0.1° Collimation	2d (Å)	13.3Å		23.6Å		44.6Å	
Crystal		I[2]	Δλ[3]	I	Δλ	I	Δλ
Mica	20.0	44	.07				
KAP	26.6	240	.07	42	.33		
OHM	63.5	24	.35	65	.80	449	1.2
Pb-Laurate	70	810	.40	1000	.49	350	1.6
Pb-Stearate	100	1000	.46	1000	.65	1000	1.7
Pb-Lignocerate	130						

[1]B. Henke and R. Lent, Some Recent Work in Low Energy X-Ray and Electron Analyses, "Advances in X-ray Analysis", Vol.12, pp. 480-495.

[2]Relative to Pb-Stearate

[3]Calculated from $\Delta\lambda = d \cos\theta \Delta(2\theta)$, where $\Delta(2\theta)$ is the full width at half maximum of the rocking curve of the crystal, including the .1° collimation.

especially since orders of reflection other than first order were used in the measurements of crystals with 2d spacings above 10Å.

5) Theoretical Studies of Optical Properties

Because of the mapping of the crystal reflection pattern, this spectrometer is extremely versatile. The detector can be placed almost anywhere, the crystal can be moved off the Rowland circle, and the x-ray lines can be observed with the crystal offset from the Bragg angle. This versatility allows the crystal and detector positions and crystal tilt to be set in order to obtain the highest efficiency and resolution for use with x-ray telescopes. Fig. 4 shows the changes in reflection pattern that result from tilting the crystal off of the Bragg angle. Computer simulations of the reflection pattern for different tilts are shown in Figs. 13, 14, and 15. Simulations corresponding to Fig. 9, which approximates the annular ring of radiation from an x-ray telescope, are shown in Figs. 16, 17 and 18. The equivalent results for a Bragg angle of 67° are shown in Figs. 19-24. Instead of being bent cylindrically, the crystal can be bent spherically to a radius R, or it can be bent cylindrically to a radius R and then ground in the plane of the bend to a radius R/2 (Johansson optics so that the planes of the crystal are bent cylindrically to a radius R and the surface of the crystal is ground to a radius R/2.

A diagram of the geometry of the spectrometer is shown in Fig. 3. If the center of the crystal is set at the Bragg angle

θ_B, then an incident ray with a horizontal divergence α and a vertical divergence ϕ strikes the crystal at an angle where

$$\Delta \approx \frac{\alpha^2}{2} \cot \theta_B - \frac{\phi^2}{2} \tan \theta_B \qquad \text{(cylindrically bent)}$$

$$\Delta \approx \frac{\alpha^2}{2} \cot \theta_B \qquad \text{(spherically bent)}$$

$$\Delta \approx - \frac{\phi^2}{2} \tan \theta_B \qquad \text{(Johansson optics).}$$

Thus, for spherical and Johansson optics, one of the aberrations is eliminated, and the reflection pattern need only be imaged with a one-dimensional array of detectors in order to obtain high spectral resolution. Simulations for spherical optics at 38° and 67° are shown in Figs. 25-38. It is, however, very difficult to properly bend crystals for spherical or Johansson optics. Only a very limited number of crystals have mechanical properties which allow these types of optics to be used. Among these crystals are LiF, which can be bent well when hot, and NaCl, which can be bent when hot or when in a saturated solution. Further investigation into these techniques and such techniques as abrasion and thermal fracturing which increase the reflectivity and rocking curve width, is needed.

Because of the α and ϕ aberrations, line radiation is not reflected from the entire crystal, thus giving rise to the reflection patterns seen in previous figures. At any one angular setting of the crystal, only a fraction F of the portion of the crystal struck by the incident annulus of radiation

is effective in Bragg reflecting that radiation. Fig. 39 gives that fraction as a function of θ_B; the half angle of the incident annulus of radiation, α; and the convolution of the crystal resolution and line width, r. This fraction F is calculated with the center of the crystal set to the Bragg angle and is the minimum efficiency that can be obtained; by setting the crystal slightly off of the Bragg angle this fraction can be increased by as much as a factor of two or three. This can be seen in Figs. 16-18, 23, 24, 28-30, and 34-38.

6) Detector Systems

A number of detector systems consistent with the requirements of the different types of focusing optics and the scientific objectives of the spectrometer have been designed and studied. These systems involve one or two-dimensional arrays consisting of proportional counters, spiraltron matrices, or image intensifiers. They are used to detect the position of x-ray events within the reflection pattern, and therefore the energy of each event.

Spherical bending of a crystal eliminates the ϕ aberration, and grinding of a crystal for Johansson optics eliminates the α aberration, so that the spectral information in the reflection pattern of the crystal is contained along a single axis. Therefore only a one-dimensional detector array is needed to obtain a high resolution spectrum. A multi-anode or multi-chamber proportional counter with an anode spacing of .025" to .040" will give a sufficiently high energy resolution.

In order to obtain high energy resolution with cylindrically bent crystals (Johann optics), two-dimensional position information is needed. The position resolution of the detector should be less than .040". (.040" corresponds to a resolution somewhat better than the natural widths of x-ray lines; high resolution studies of doppler broadening and shifts will require a position resolution about a factor of two better than this). A multi-anode proportional counter in which the anodes are constructed of a resistive material such as 1 mil nichrome (20 ohms/cm) may provide approximately this resolution. The ratio of the charges collected by preamplifiers on both ends of the anode can be used to determine the position of the incident x-ray along the length of the anode. The positions of x-ray events can also be obtained through the use of a spiraltron matrix[5] and position detection electronics, or an image intensifier with a fluorescent screen and a vidicon. A spiraltron bundle is a matrix of spiraltrons, each consisting of six small channel electron multiplier tubes wound around a central core. It has inherently good position resolution (about .003") and high gain (10^7 to 10^8).

One method of detecting the position of each event is to place a fluorescent screen behind the spiraltron bundle (see Fig. 40). The electron pulse striking the screen will produce an easily detectable spot of light. The coordinates of this spot can be obtained by placing a one-dimensional array of photodiodes or phototransistors at the focus of each of a pair of cylindrical lenses. A bean splitter will transfer

half of the light to each lens; one lens will focus the light into a vertical line and the other, into a horizontal line. The position of the spot of light along each focus gives one of the coordinates of the event.

Another position detection scheme is to place two grids of wires, one behind the other and oriented at right angles to each other, behind the matrix of spiraltrons (Fig. 41). Preamplifiers would be connected to the end of each wire. An electron pulse would be detected by one wire of each grid, thus giving the coordinates of that event.

A final detection system consists of a spiraltron matrix or an image intensifier with a fluorescent screen and a high sensitivity vidicon, such as an SEC vidicon, which provides an image of the screen (Fig. 42).

Of these detection schemes, the proportional counter systems are probably most efficient (about 30-60% for 15Å to 4Å x-rays). Because the photocathodes must be very thin, the spiraltron matrices would require photocathodes deposited right on the surface, or preferably inside the tubes, since photocathodes are more efficient at small angles of incidence. At 8Å, CsI efficiencies vary from about 30% at 90° angle of incidence to near 100% at 5°. These efficiencies are less for higher energy x-rays. Several other systems which may possibly have a high detection efficiency are being investigated. One of these consists of a transparent fluorescent material which converts an incident x-ray into a number of optical photons which then strike a photocathode placed in

front of a spiraltron matrix. Finally, the image intensifier and vidicon system has been built and tested by several groups working in the optical region, so that its properties are known but its time resolution (at 60 frames per second) is only 16 msec, thus making fast pulsar studies impossible. All of the other systems have inherent time resolutions of less than 1 μsec.

7) X-Ray Collector Definition

In a series of meetings with the American Science and Engineering, Columbia, and Goddard groups, the nature and requirements of the spectrometer were presented, along with several ideas and designs for related ancillary experiments. This has led to discussions on the performance and design of the x-ray collectors and the interrelationship of the various experiments with each other and the collectors. Some of the results of these meetings are put forth in a joint report of the x-ray astronomy groups at AS&E, Columbia, Goddard, and MIT[1].

References

1. Preliminary Study: Telescopes and Scientific Subsystems for a High Energy Astronomy Observatory, ASE-2266-A

2. H. W. Schnopper and K. Kalata, App. Phys. Lett. 15, 134 (1969)

3. H. W. Schnopper and K. Kalata, Astron. J. 74, 854 (1969)

4. Application # 825532, A High-Dispersion, High-Resolution Spectrometer

5. T. A. Somer and P. W. Graves, IEEE Transactions on Nuclear Science, NS-16, 1, 376 (1969)

Figure Captions

Fig. 1. A photograph of the x-ray spectrometer system, including the vacuum system for the x-ray tube and some of the related electronics.

Fig. 2. A close-up of the x-ray spectrometer.

Fig. 2a. An overlay for Fig. 2 showing the various components of the spectrometer and its mechanical motions.

1. x-ray tube, 2. location of x-ray port and interchangeable window, 3. removable electron gun, 4. proportional counter with pinhole aperature, 5. crystal holder, 6. micrometer for inclining the crystal relative to the vertical direction, 7. micrometer for moving the crystal along the direction normal to the crystal surface, 8. x-z table driven by stepping motors 9 and 10 for positioning and scanning the detector across the crystal reflection pattern, 11. rotary table for setting the crystal to the proper angular setting, 12. rotary table for setting the detection arm, 16, to the proper angular setting, 13. stepping motor which drives a precision micrometer, 14, which in turn finely adjusts a tangent arm attached to the crystal table and scans the crystal angle around the Bragg angle, 15. movable table which adjusts the distance from the point source of x-rays to the crystal, 16. the detection arm which moves the detector and its x-z table to or away from the focus, 17. preamplifier for the proportional counter.

Fig. 3. X-ray pictures of the $CuK\alpha_1\alpha_2$ doublet in 8th order after Bragg reflection from a cylindrically bent mica crystal with a radius of 10". The film was placed

3 1/8" from the crystal and the exposure was 10 min at 1 ma and 20kv, The $K\alpha_1$ reflection pattern can be recognized because it is twice as intense as that of $K\alpha_2$. The approximate angular difference between the crystal angle and the Bragg angle is a) 11', b) 6', c) 0', d) -8'.

Figs. 5-9 were all taken at 20kv and 1.4 ma.

Fig. 5. Two x-ray pictures of the reflection pattern LiF of CuKα radiation in second order, taken at 49.9° (b) and 50.0° (a) in a 30 min exposure.

Fig. 6. An X-ray picture of the 15th order reflection pattern of CuKα radiation from OHM. The line at bottom left is the reflection pattern, the pattern at top right is from another set of planes in the OHM. The exposure was 30 min.

Fig. 7. X-ray pictures of the 4th order reflection pattern of CuKα radiation from ADP. The angular settings of the crystal were a) 35°, b) 35.5°, c) 36°. 30 min exposure were used.

Fig. 8. X-ray pictures of the 7th order reflection from KAP of CuKα radiation taken with 45 min exposures. The angular settings were a) 26.5°, b) 25.5°, c) 24.5°

Fig. 9. X-ray pictures of the 8th order reflection pattern of CuKα radiation from mica with 20 min exposures. A annulus of radiation with a 10° outer diameter and a 1° width was used. The angular settings of the crystal were a) 39.1° b) 38.95° c) 38.8° d) 38.65°

Fig. 10. A graph of the peak reflectivity of a KAP crystal vs. wavelength of the incident x-rays.

Fig. 11. A graph of the rocking width at half maximum of a KAP crystal in seconds of arc vs. wavelength.

Fig. 12. A graph of the rocking curve width at half maximum of a KAP crystal in electron volts vs. wavelength.

Figs.13-38. are computer simulations of the reflection pattern of $CuK\alpha_1\alpha_2$ radiation from cylindrically bent (13-25) crystals with a 10° cone of incident radiation. The Bragg angle is θ_B, the distance from the source to the crystal is 10", the distance from the crystal to the detector plane is 3 1/8", and the convolution of the natural line width and the crystal resolution is 2500. The difference between the angular setting of the crystal and the Bragg angle, TILT, is given in minutes of arc. In Figs. 16-18, 23, 24, 28-30, and 35-38 and annulus of incident radiation 10° in outer diameter and 1° wide was used.

Fig. 39. A graph of the efficiency F for reflecting an x-ray line from cylindrically bent and spherically bent crystals for the cases when all of the radiation falls on an annulus of negligable width and 2° and 5° in half angle. This quantity is obtained by calculating what fraction of the incident radiation strikes a portion of the crystal where the quantity $|\Delta|$ is less than $\Delta_{1/2} = \frac{\tan \theta_B}{r}$. r is the convolution of the natural line width and the crystal resolution.

Figs.40-42 Three different detection systems which detect the position of each incident x-ray.

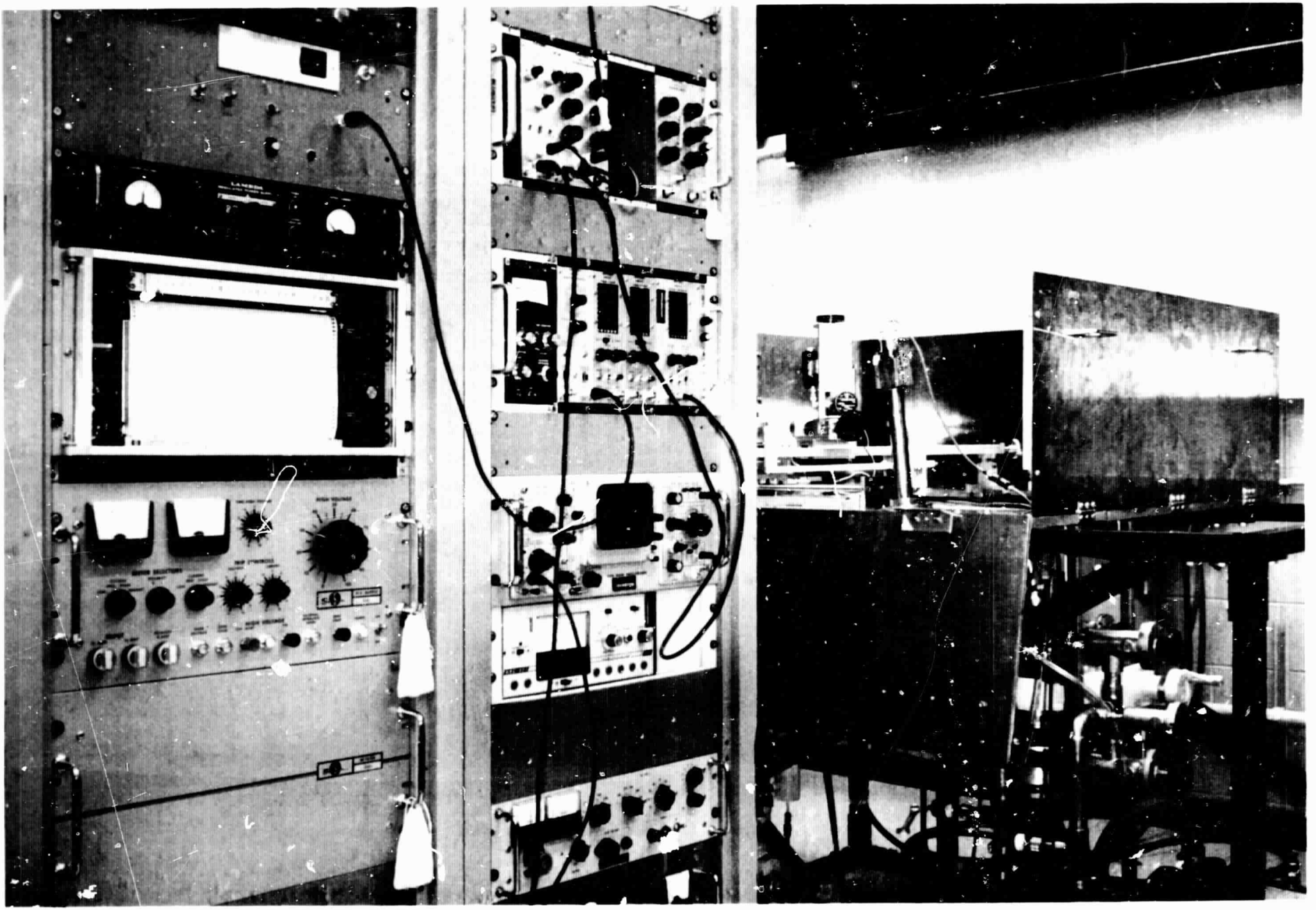

Fig. 1

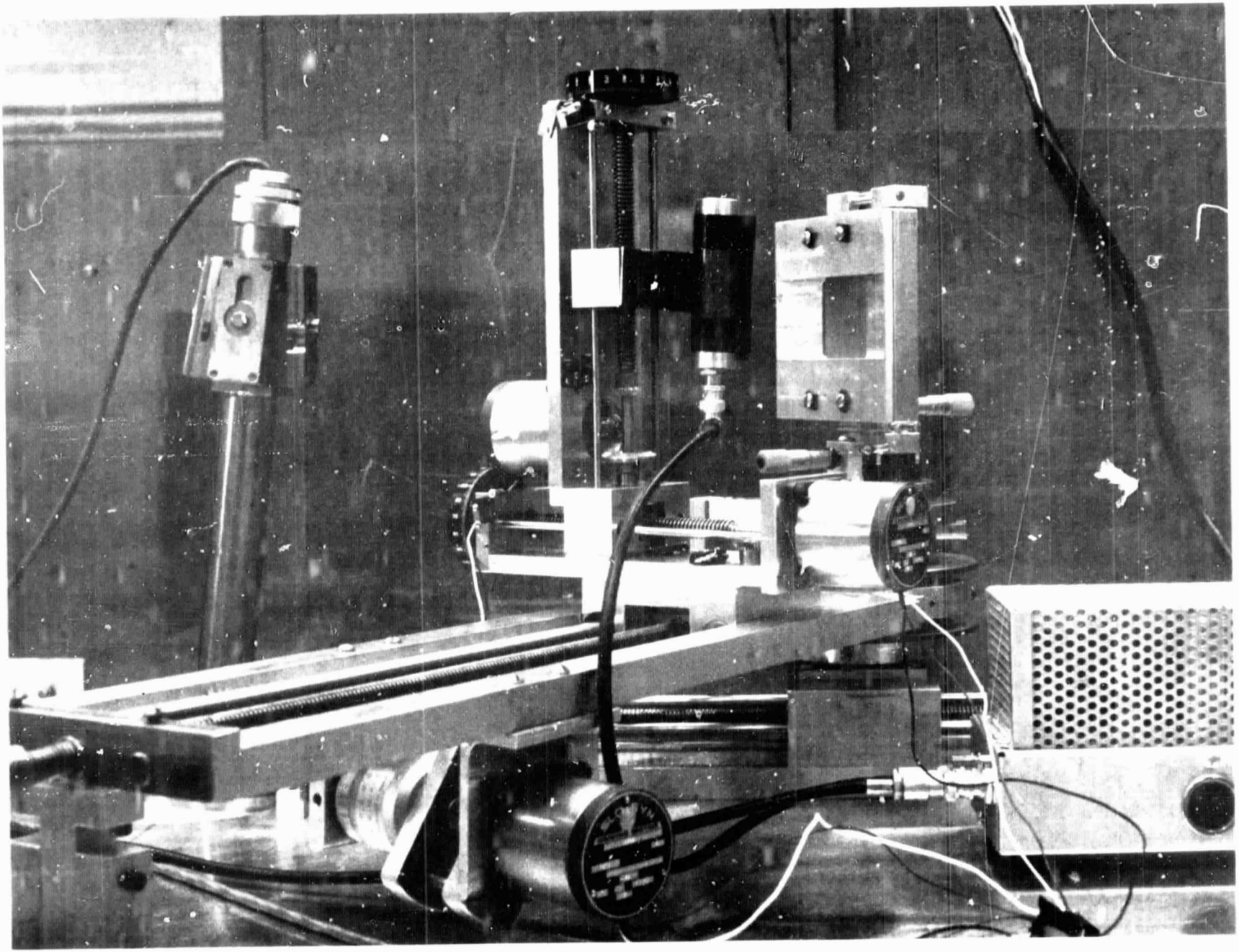

Fig. 2

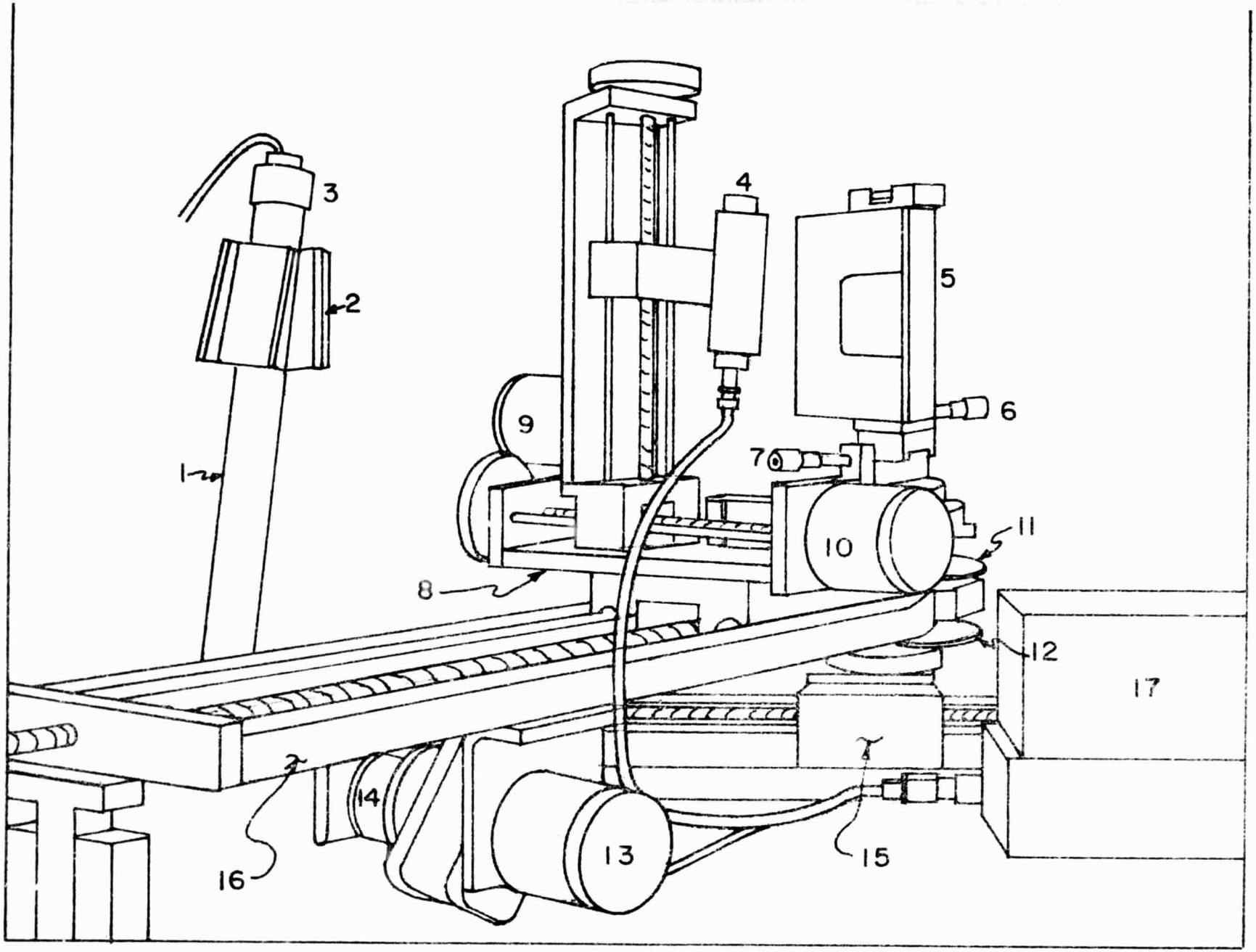

Fig. 2a

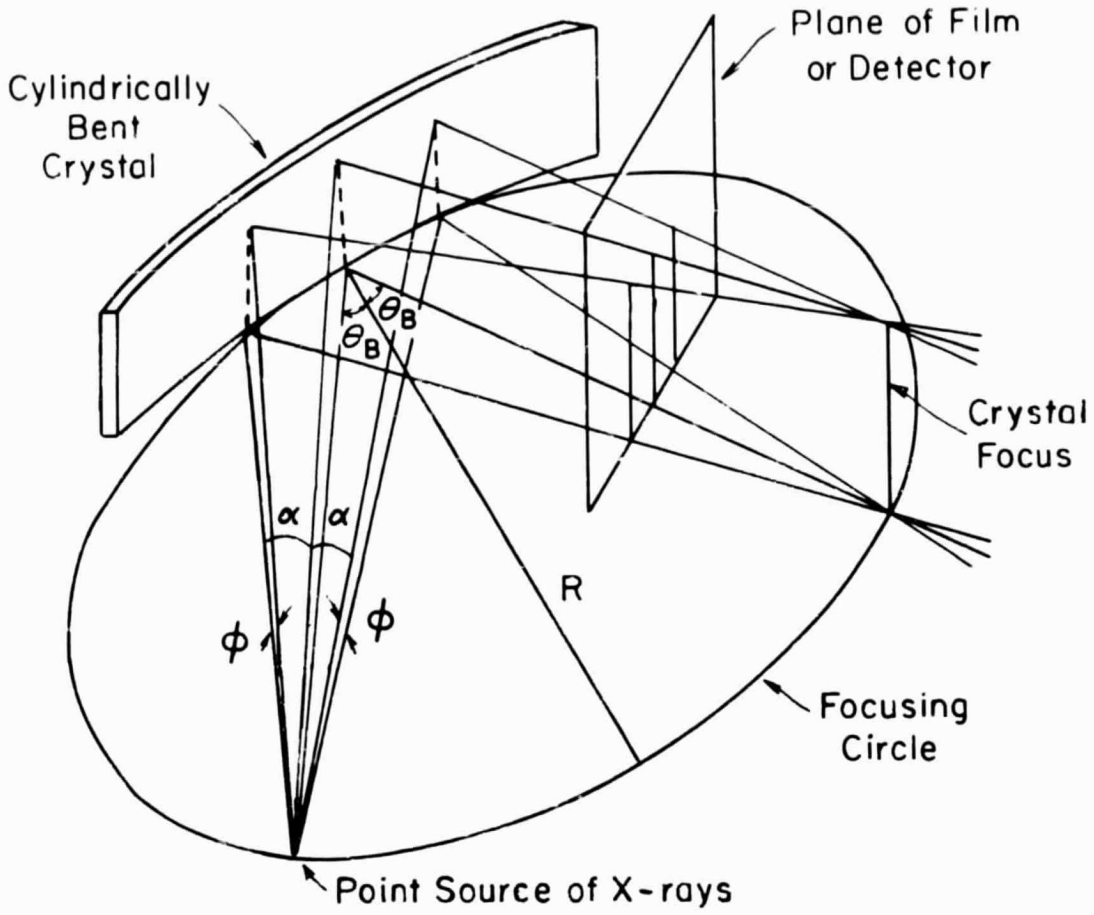

Fig. 3

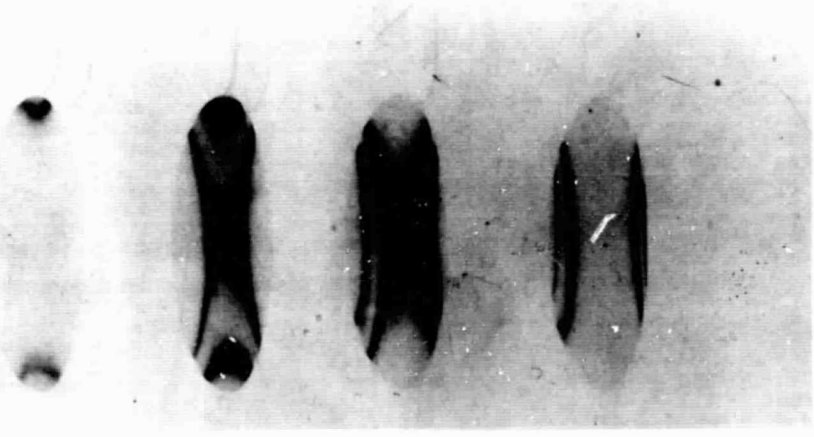

a b c d

Fig. 4

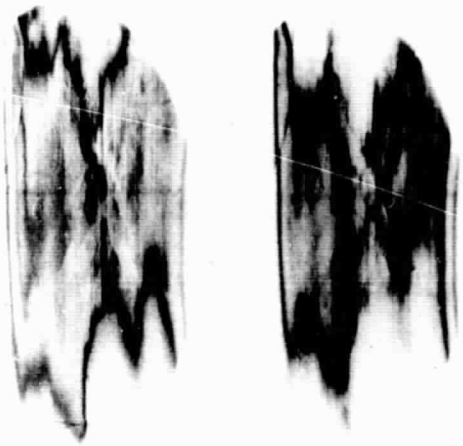

a b

Fig.5

Fig.6

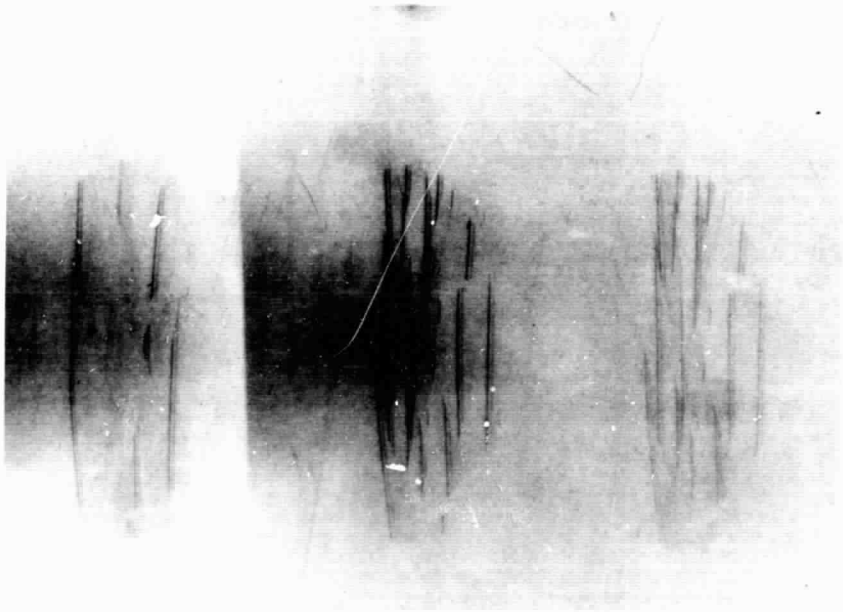

a b c

Fig.7

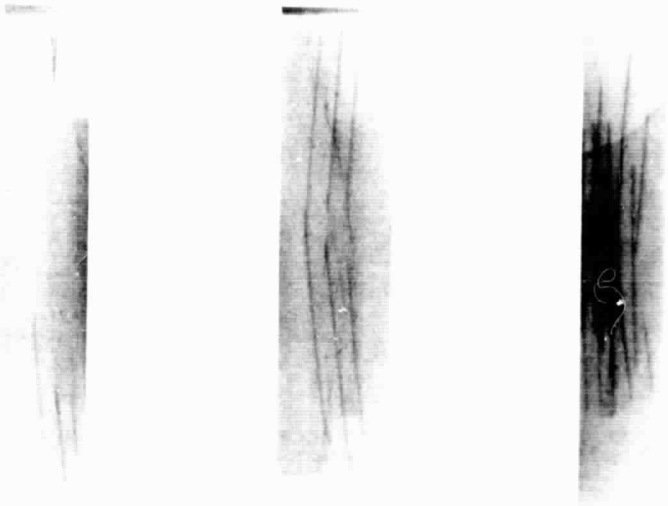

a b c

Fig. 8

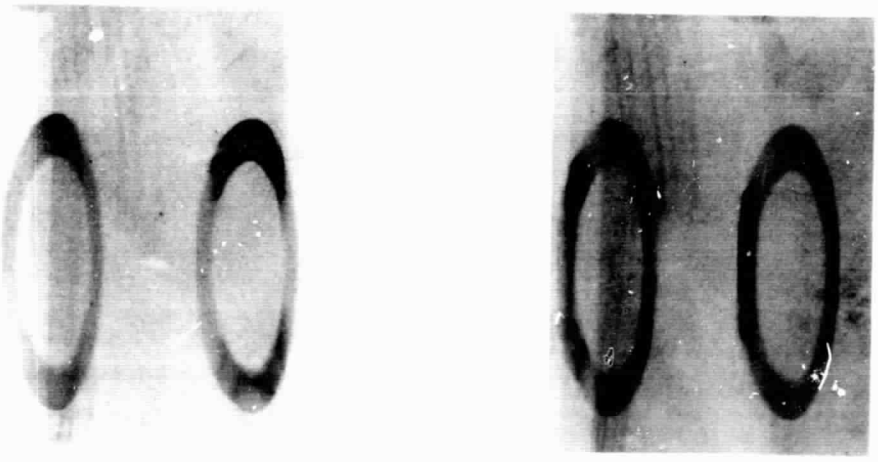

a b c d

Fig. 9

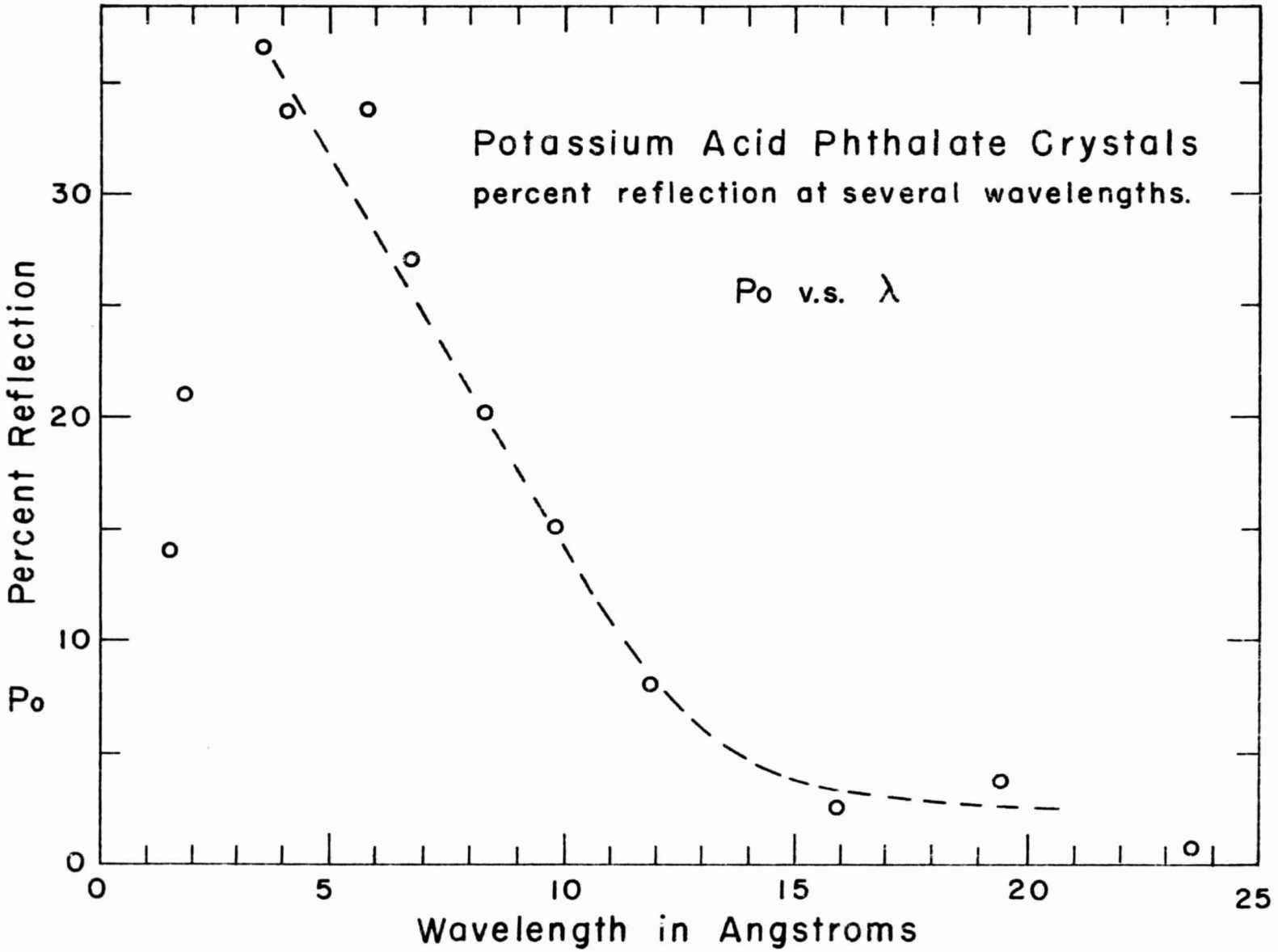
Potassium Acid Phthalate Crystals
percent reflection at several wavelengths.
Po v.s. λ
Percent Reflection
Po
0
10
20
30
0
5
10
15
20
25
Wavelength in Angstroms

Fig. 10

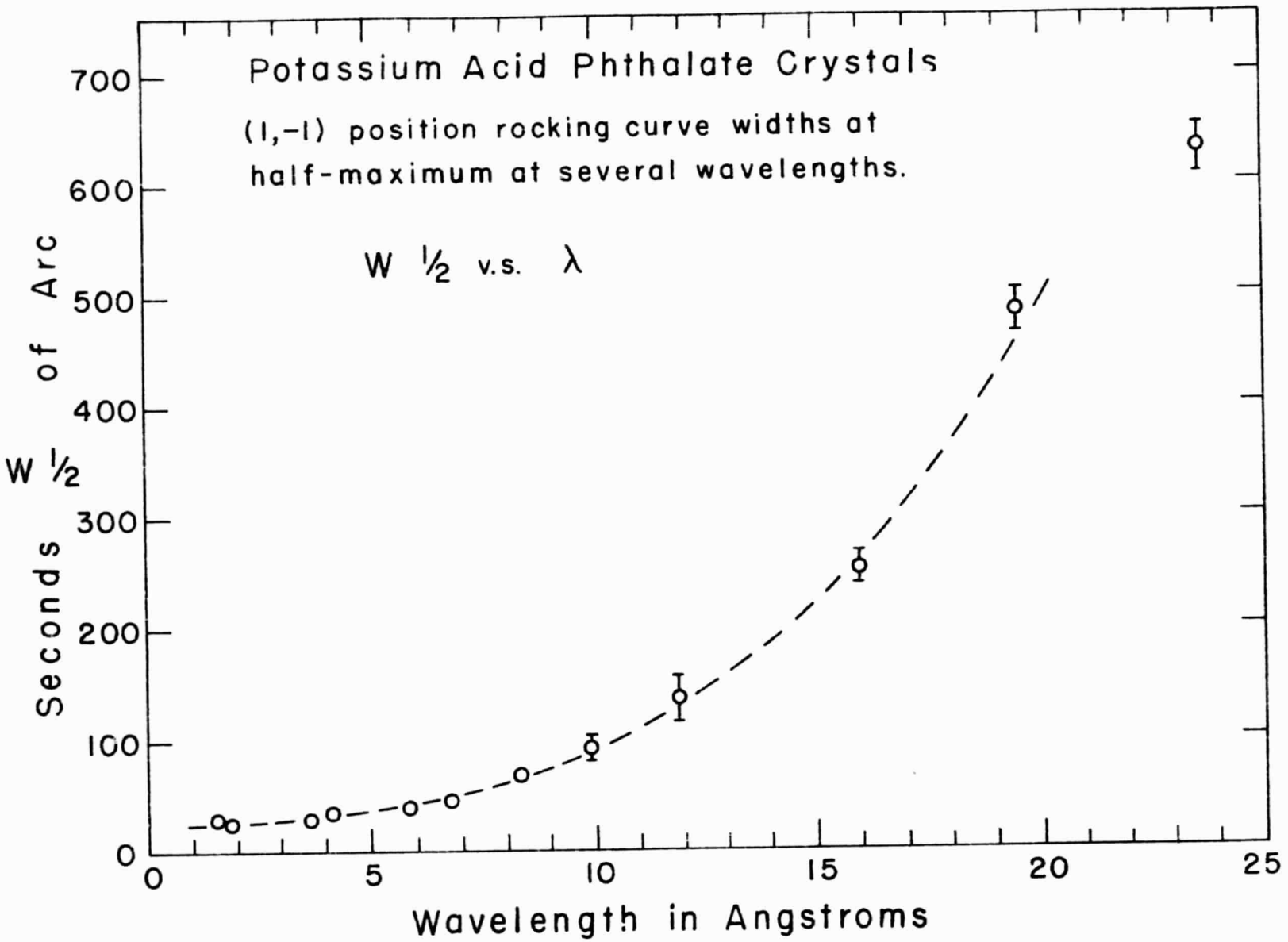
Potassium Acid Phthalate Crystals
(1,-1) position rocking curve widths at
half-maximum at several wavelengths.
W ½ v.s. λ
W ½
Seconds of Arc
0
100
200
300
400
500
600
700
0
5
10
15
20
25
Wavelength in Angstroms

Fig. II

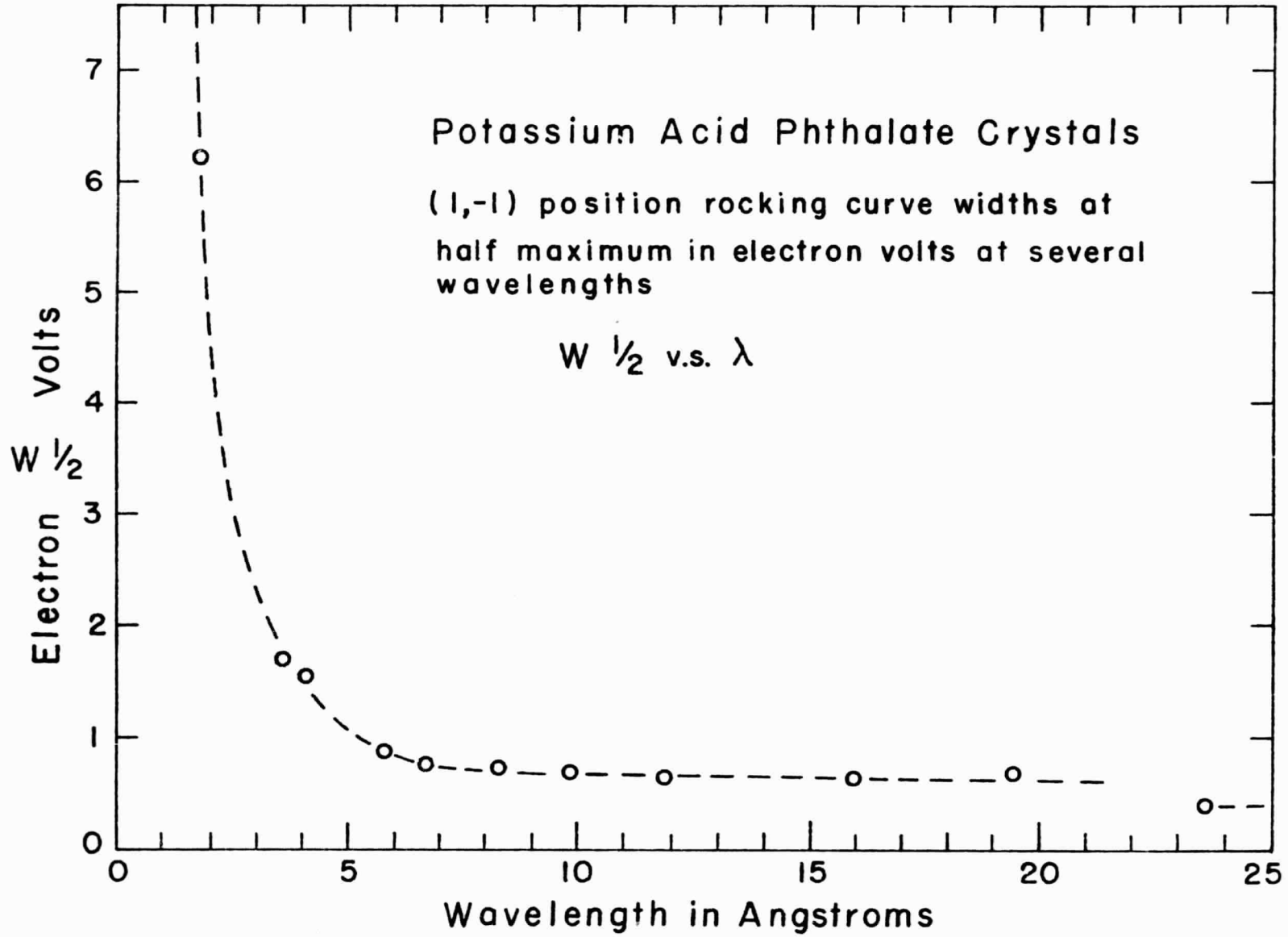
Potassium Acid Phthalate Crystals
(1,-1) position rocking curve widths at half maximum in electron volts at several wavelengths
W ½ v.s. λ
Electron Volts
W ½
0
1
2
3
4
5
6
7
0
5
10
15
20
25
Wavelength in Angstroms

Fig. 12

6.0 ° TILT $\theta_B = 38°$ SOURCE SHIFT ↓ 0.000 "

R=10.00 R1=3.13 RES=2500. TILT2=0.5

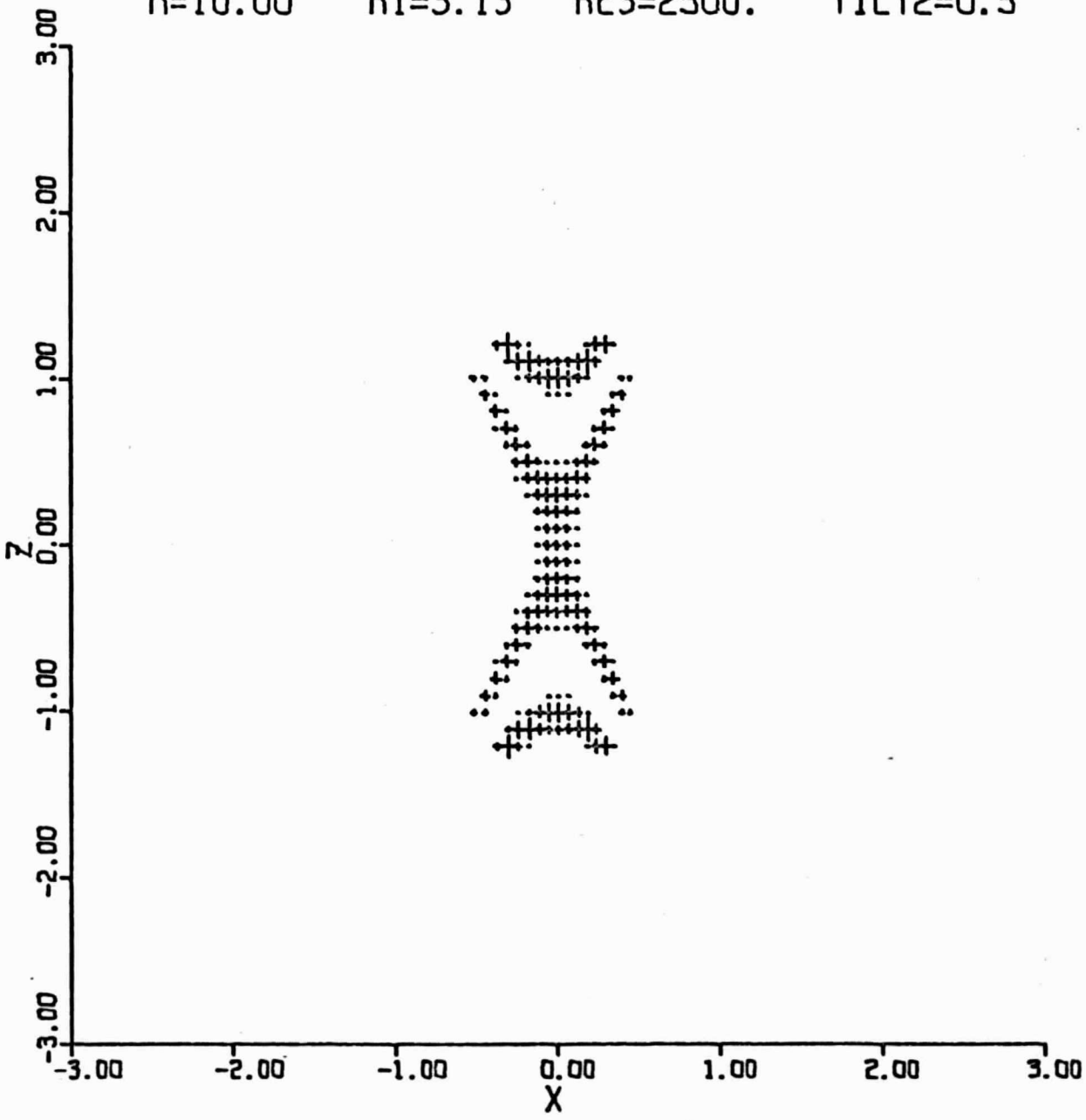

Fig 13

0.0 ° TILT $\theta_B = 38^\circ$ SOURCE SHIFT ↓ 0.000 "

R=10.00 R1=3.13 RES=2500. TILT2=-5.5

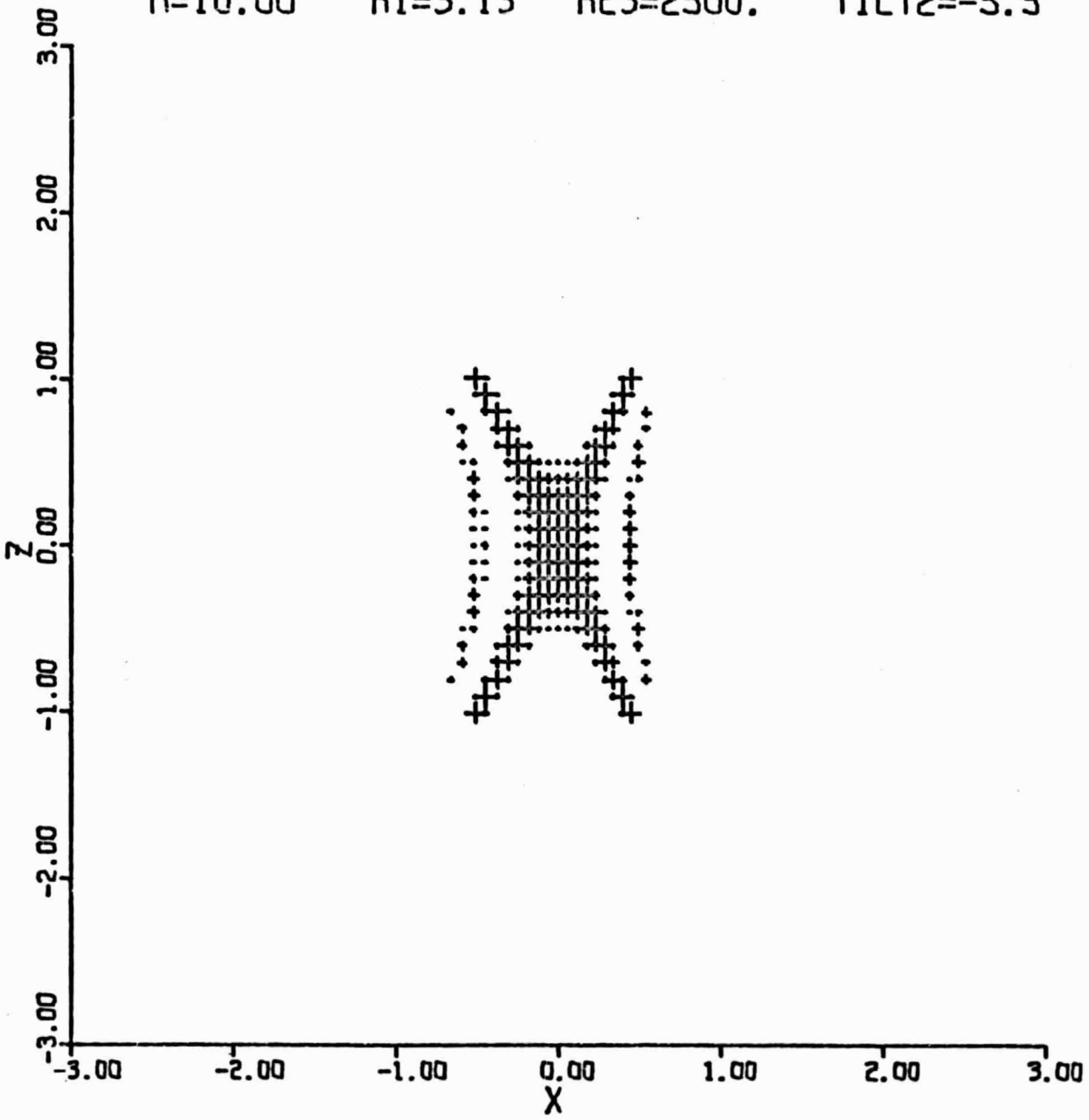

Fig 14

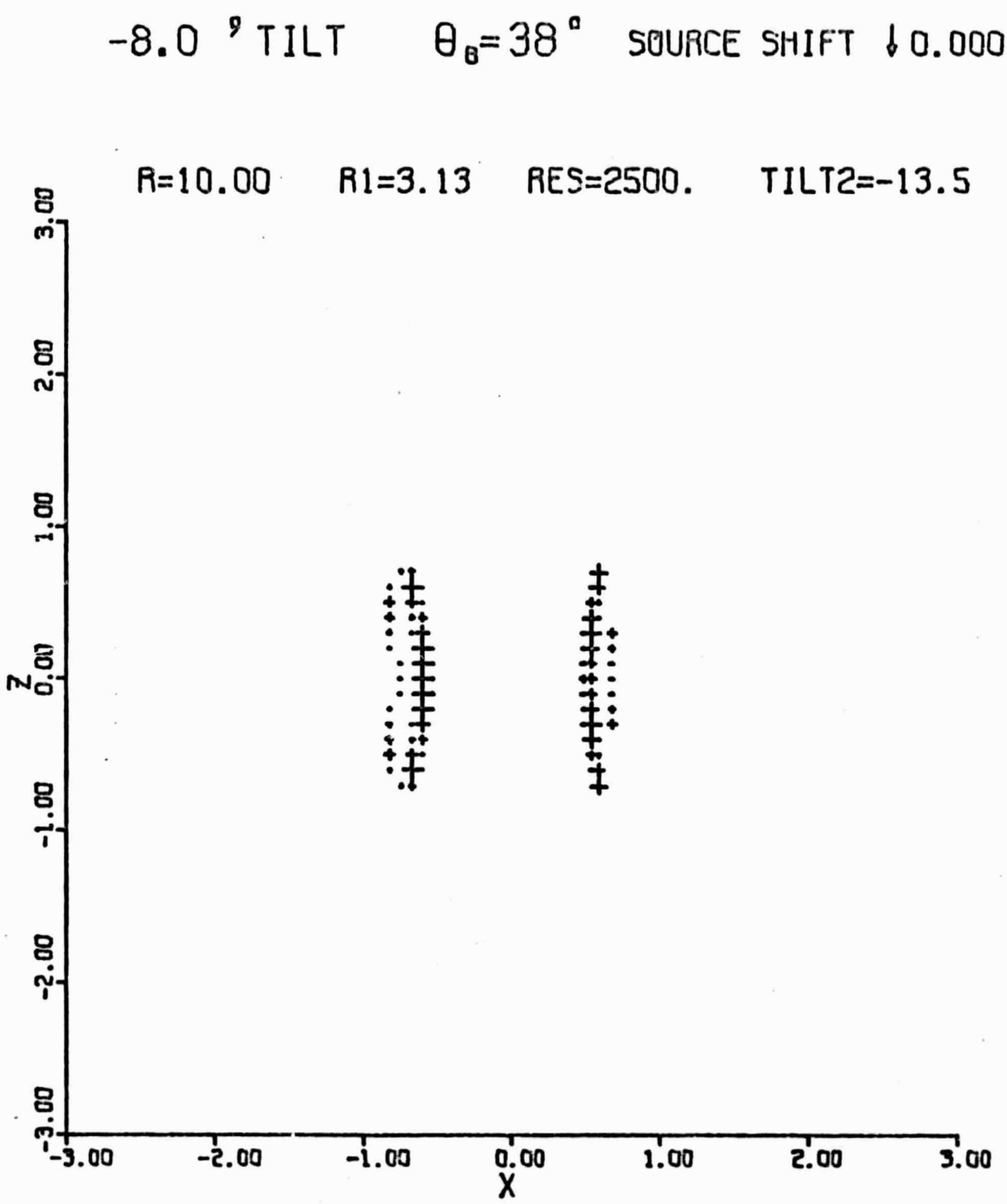
-8.0 ° TILT
θB=38°
SOURCE SHIFT ↓0.000 "
R=10.00
R1=3.13
RES=2500.
TILT2=-13.5
3.00
2.00
1.00
0.00
-1.00
-2.00
-3.00
Z
-3.00
-2.00
-1.00
0.00
1.00
2.00
3.00
X

Fig 15

6.0 ° TILT $\theta_B = 38°$ SOURCE SHIFT ↓ 0.000 "

R=10.00 R1=3.13 RES=2500. TILT2=0.5

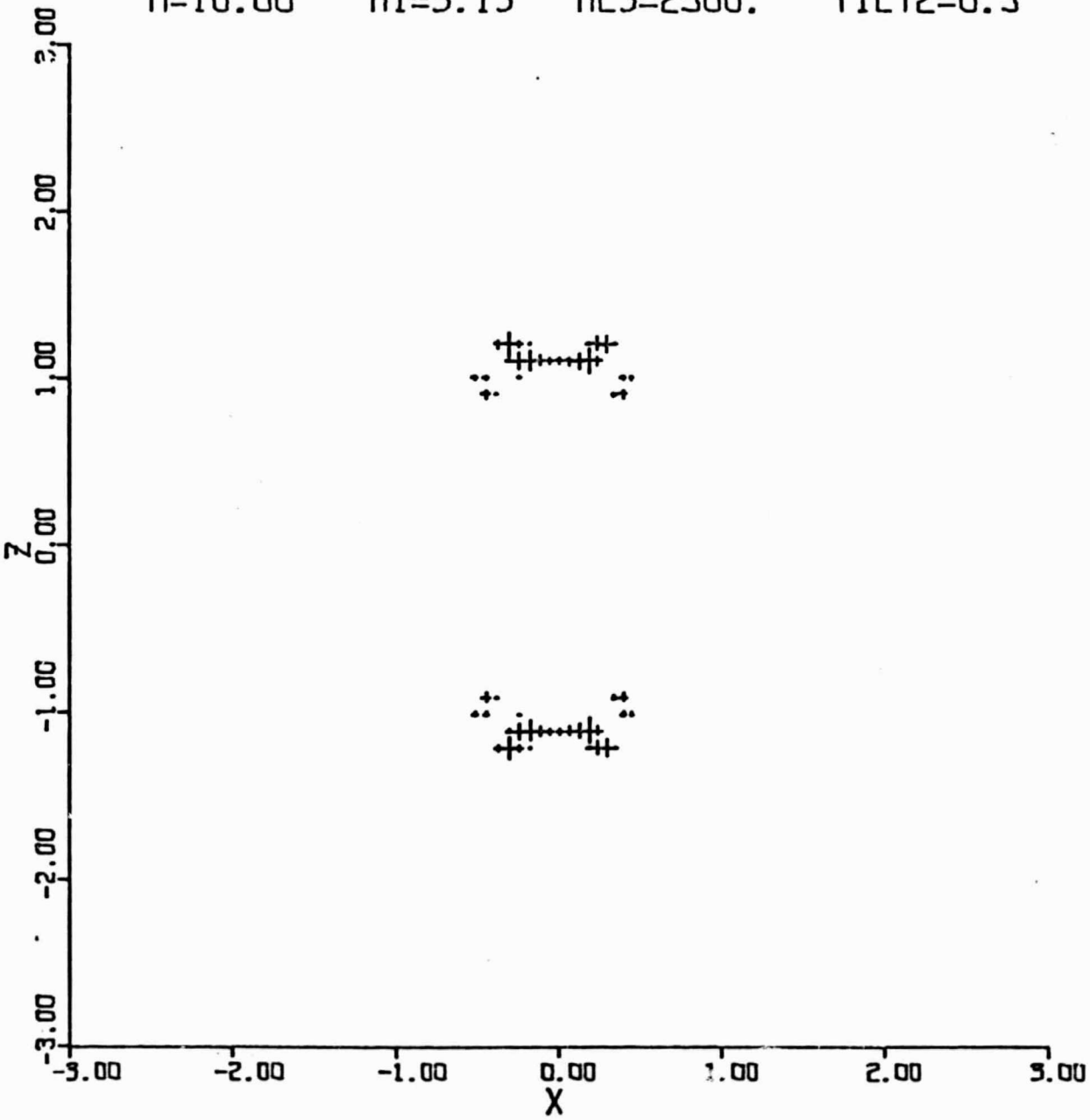

Fig 16

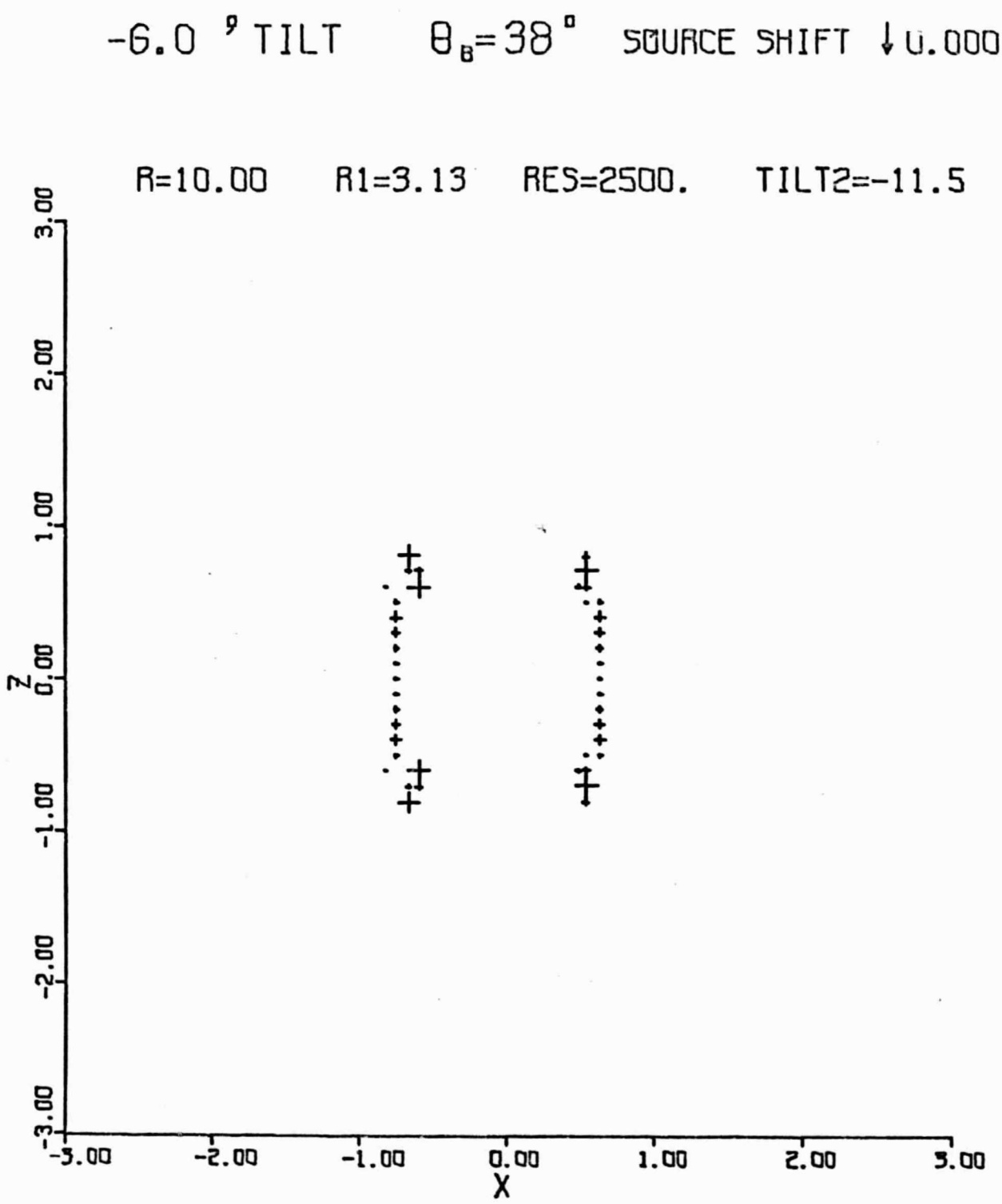
-6.0 ° TILT
θB=38°
SOURCE SHIFT ↓0.000
R=10.00
R1=3.13
RES=2500.
TILT2=-11.5
3.00
2.00
1.00
0.00
-1.00
-2.00
-3.00
Z
-3.00
-2.00
-1.00
0.00
1.00
2.00
3.00
X

Fig 17

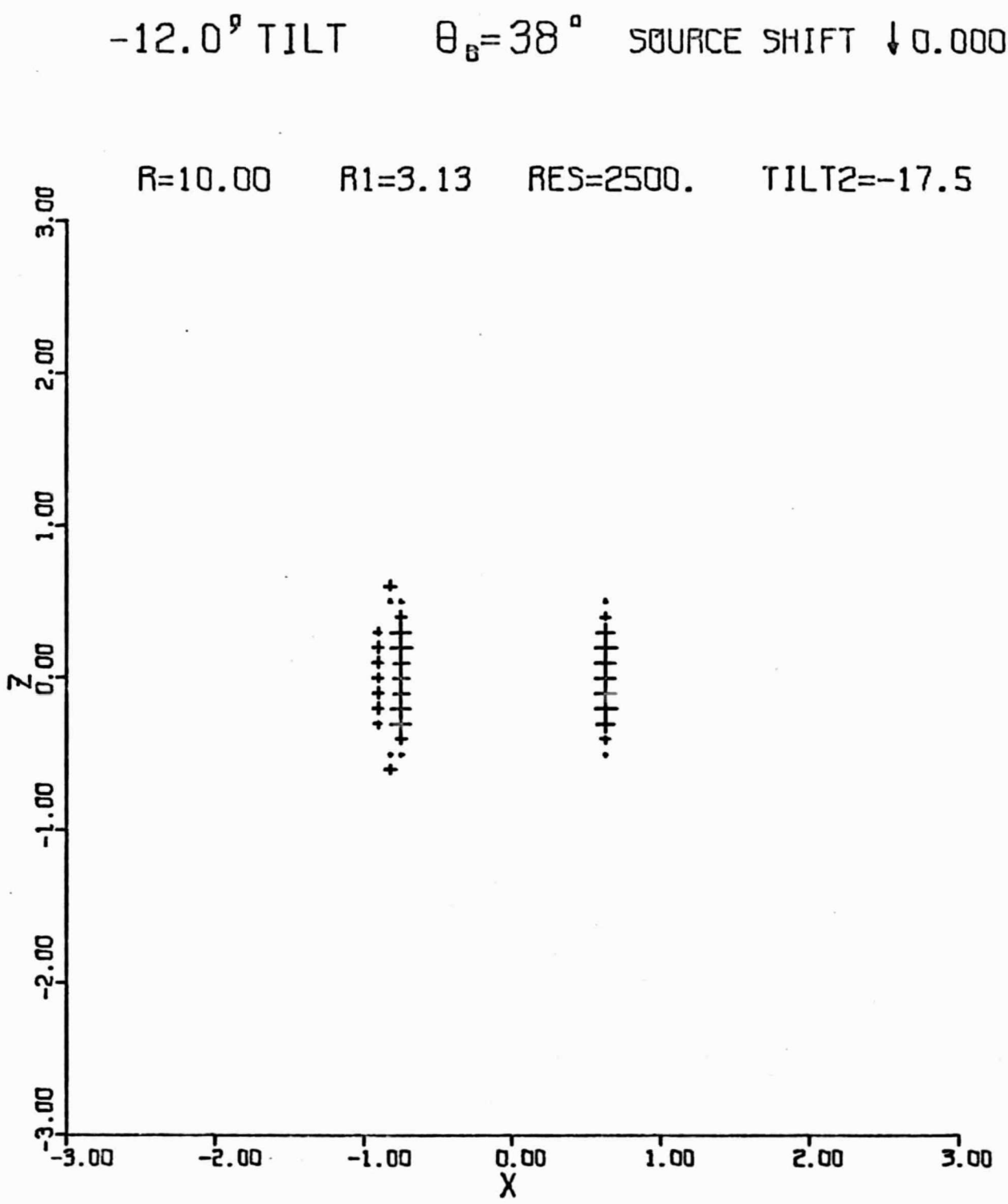
-12.0° TILT
θB=38°
SOURCE SHIFT ↓0.000
R=10.00
R1=3.13
RES=2500.
TILT2=-17.5
3.00
2.00
1.00
0.00
-1.00
-2.00
-3.00
Z
-3.00
-2.00
-1.00
0.00
1.00
2.00
3.00
X

Fig 18

12.0 ° TILT θ_B=67° SOURCE SHIFT ↓0.000 "

R=10.00 R1=3.13 RES=2500. TILT2=0.9

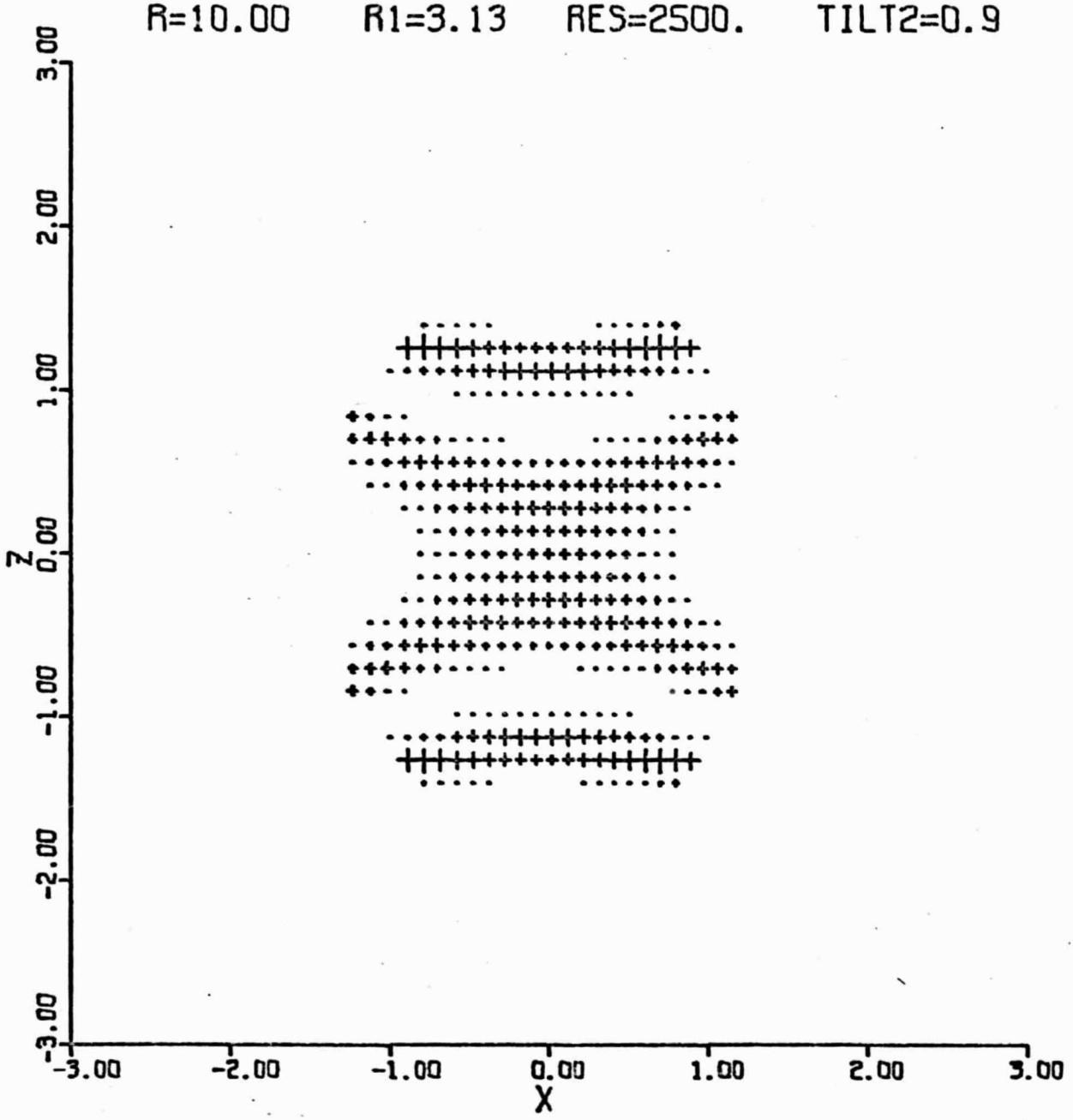

Fig 19

8.0 ° TILT θ_0=67° SOURCE SHIFT ↓0.000 "

R=10.00 R1=3.13 RES=2500. TILT2=-3.1

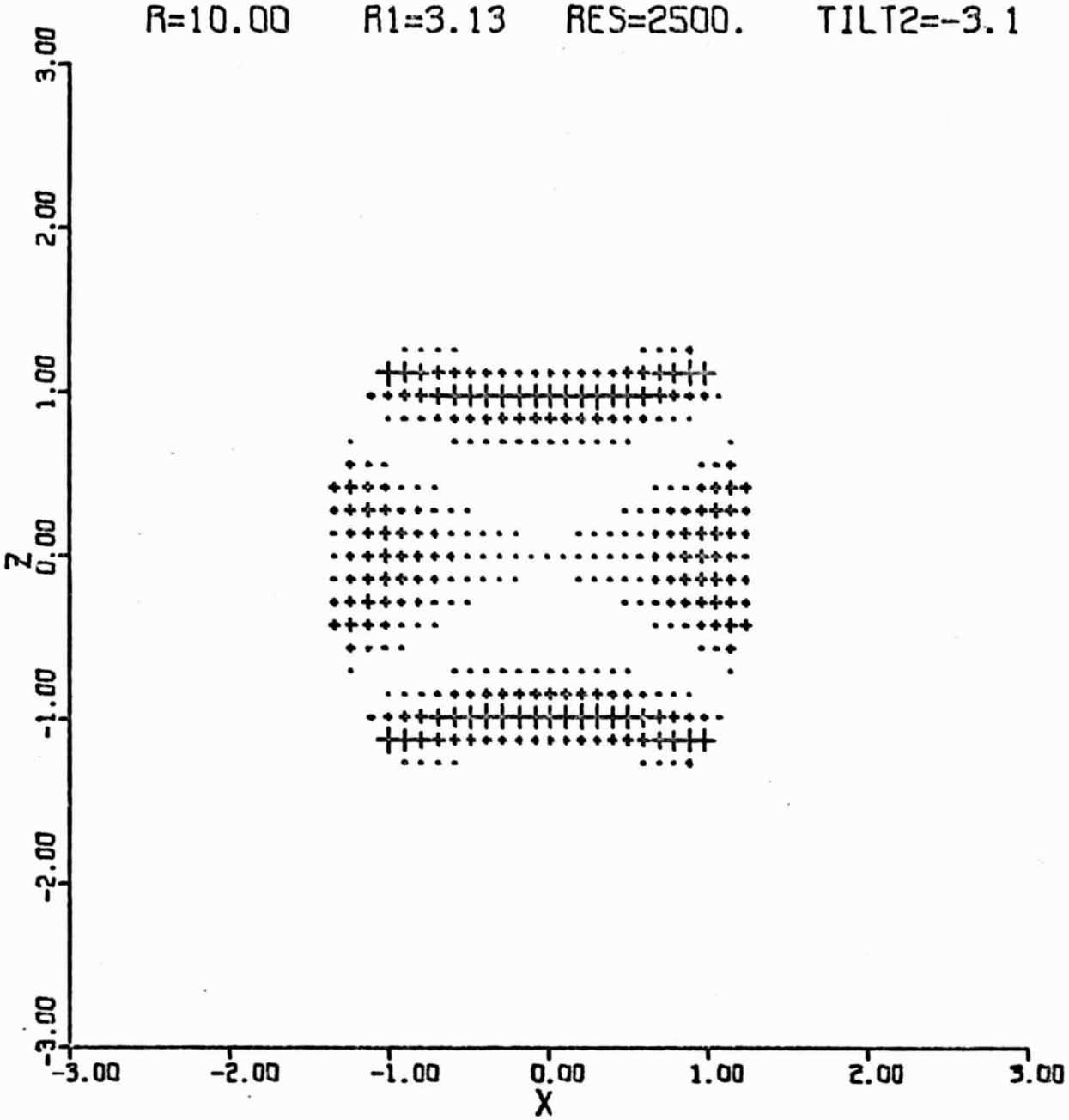

Fig 20

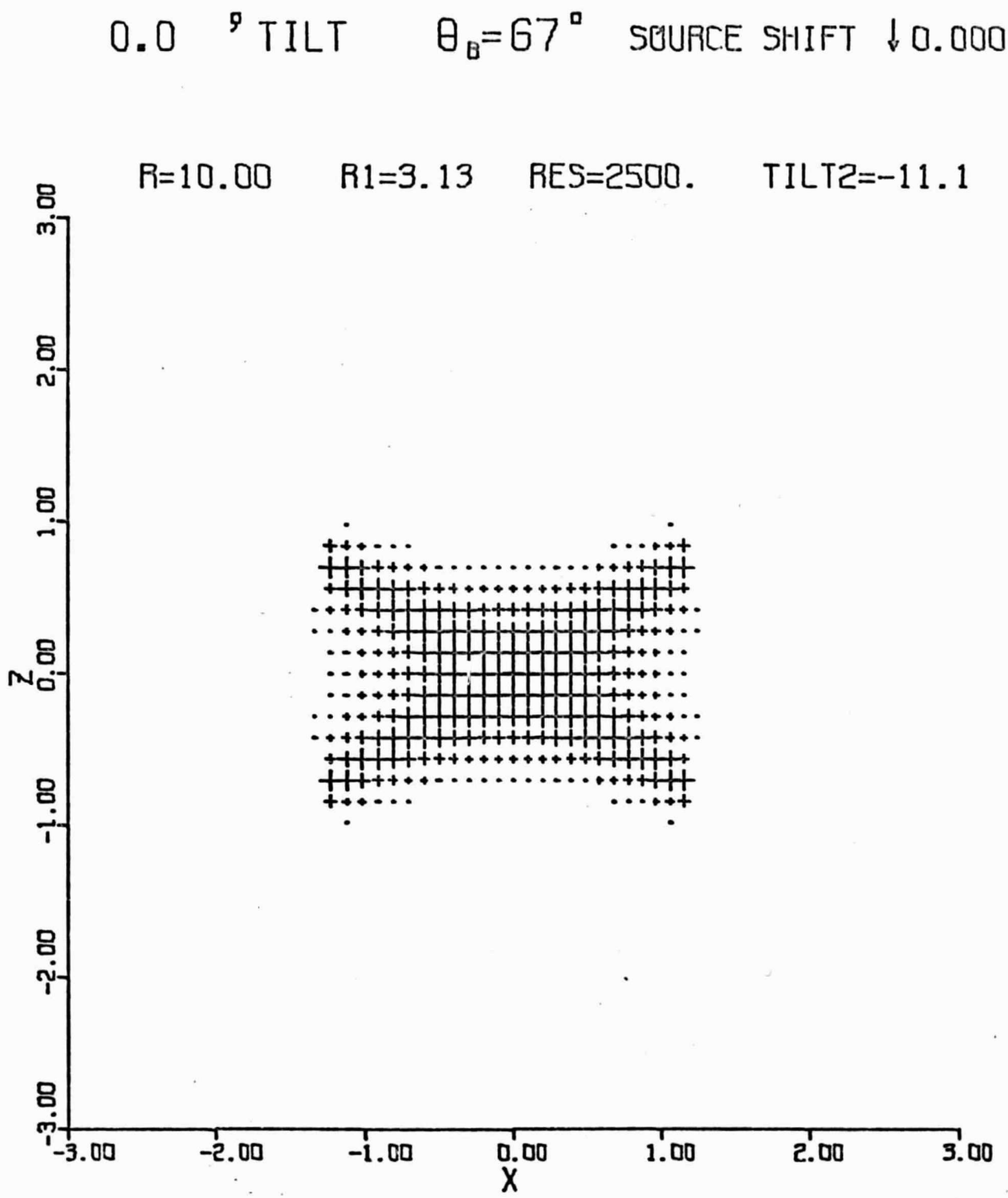
0.0 ° TILT θ_B=67° SOURCE SHIFT ↓0.000 "
R=10.00 R1=3.13 RES=2500. TILT2=-11.1
3.00
2.00
1.00
0.00
-1.00
-2.00
-3.00
Z
-3.00
-2.00
-1.00
0.00
1.00
2.00
3.00
X

Fig 21

-4.0 ° TILT θ_B=67° SOURCE SHIFT ↓0.000 "

R=10.00 R1=3.13 RES=2500. TILT2=-15.1

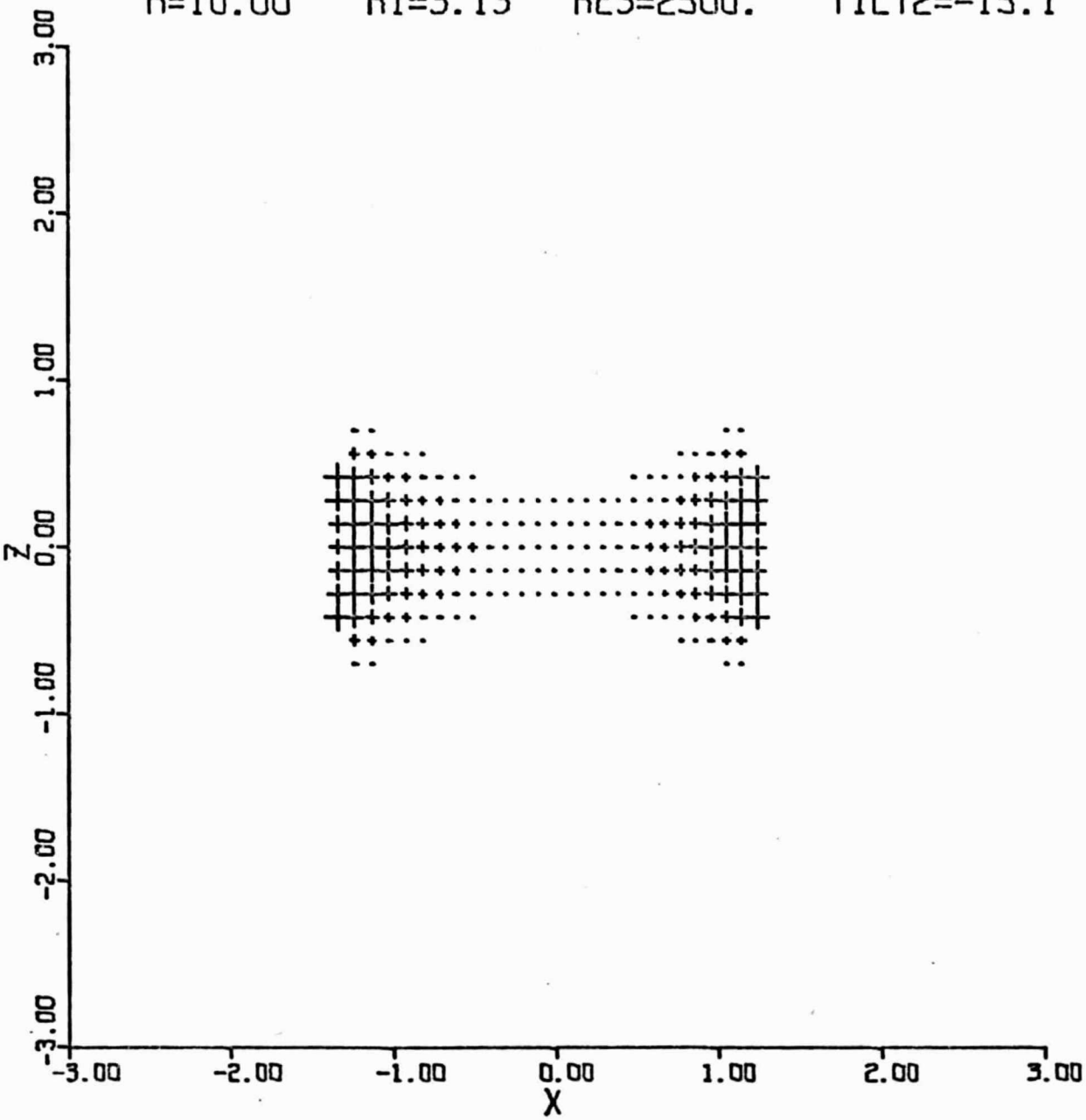

Fig 22

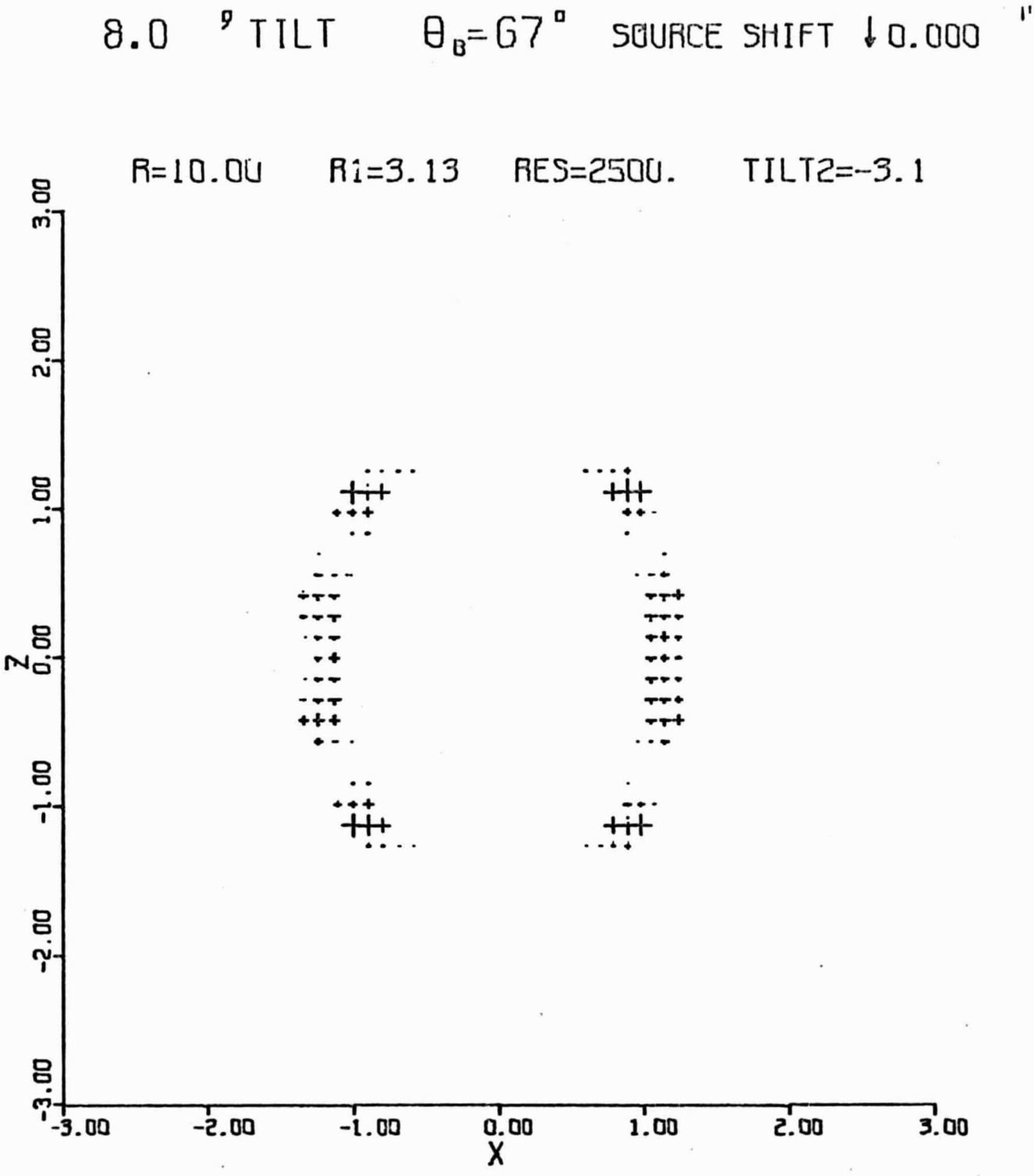
8.0 ' TILT θ_B=67° SOURCE SHIFT ↓0.000 "
R=10.00 R1=3.13 RES=2500. TILT2=-3.1
3.00
2.00
1.00
0.00
-1.00
-2.00
-3.00
Z
-3.00
-2.00
-1.00
0.00
1.00
2.00
3.00
X

Fig 23

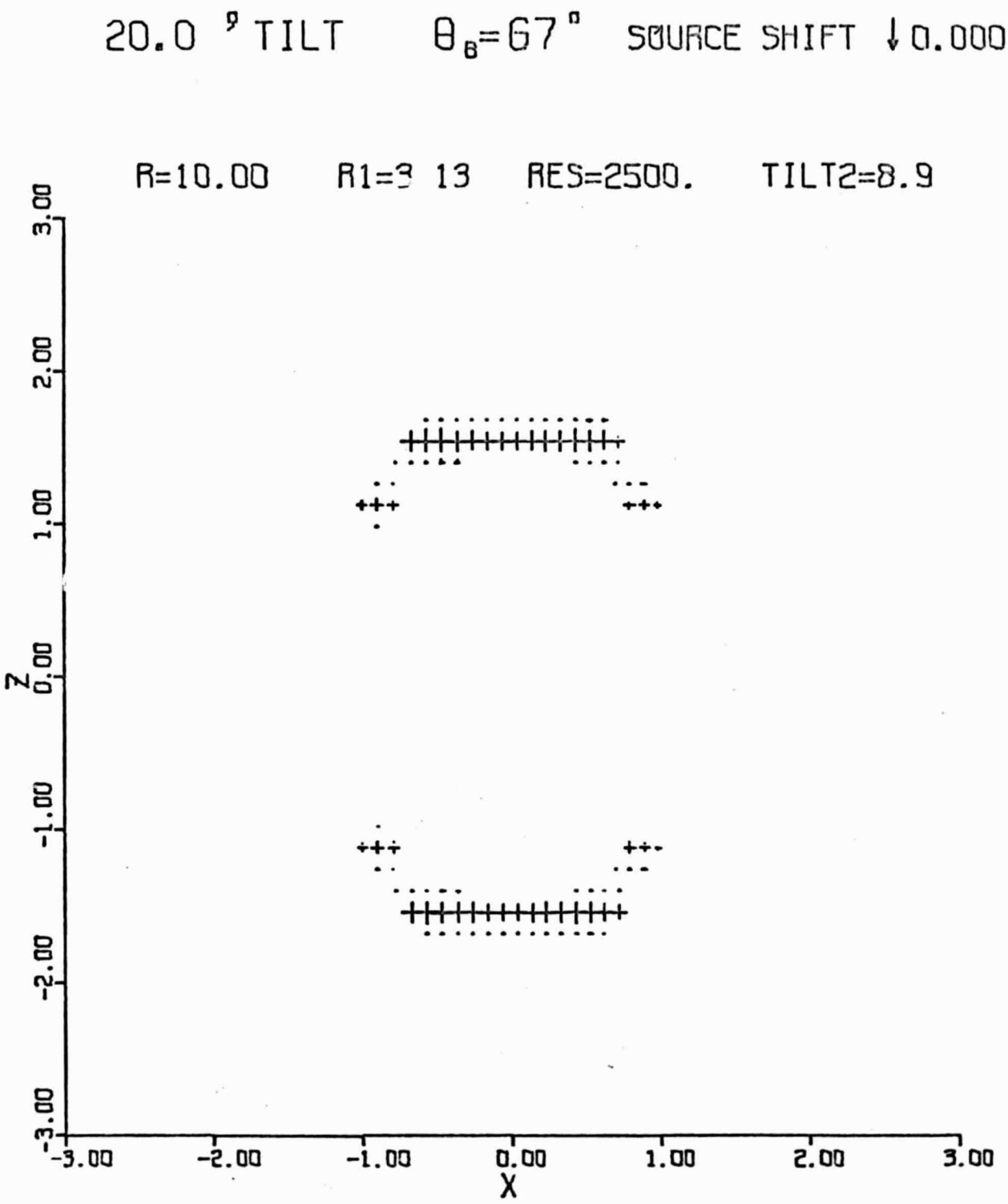
20.0 ° TILT θ_B=67° SOURCE SHIFT ↓0.000 "
R=10.00 R1=3 13 RES=2500. TILT2=8.9
3.00
2.00
1.00
0.00
-1.00
-2.00
-3.00
Z
-3.00
-2.00
-1.00
0.00
1.00
2.00
3.00
X

Fig 24

0.0 ° TILT $\theta_B = 38°$ SOURCE SHIFT ↓ 0.000 "

R=10.00 R1=3.13 RES=2500. TILT2=-5.5

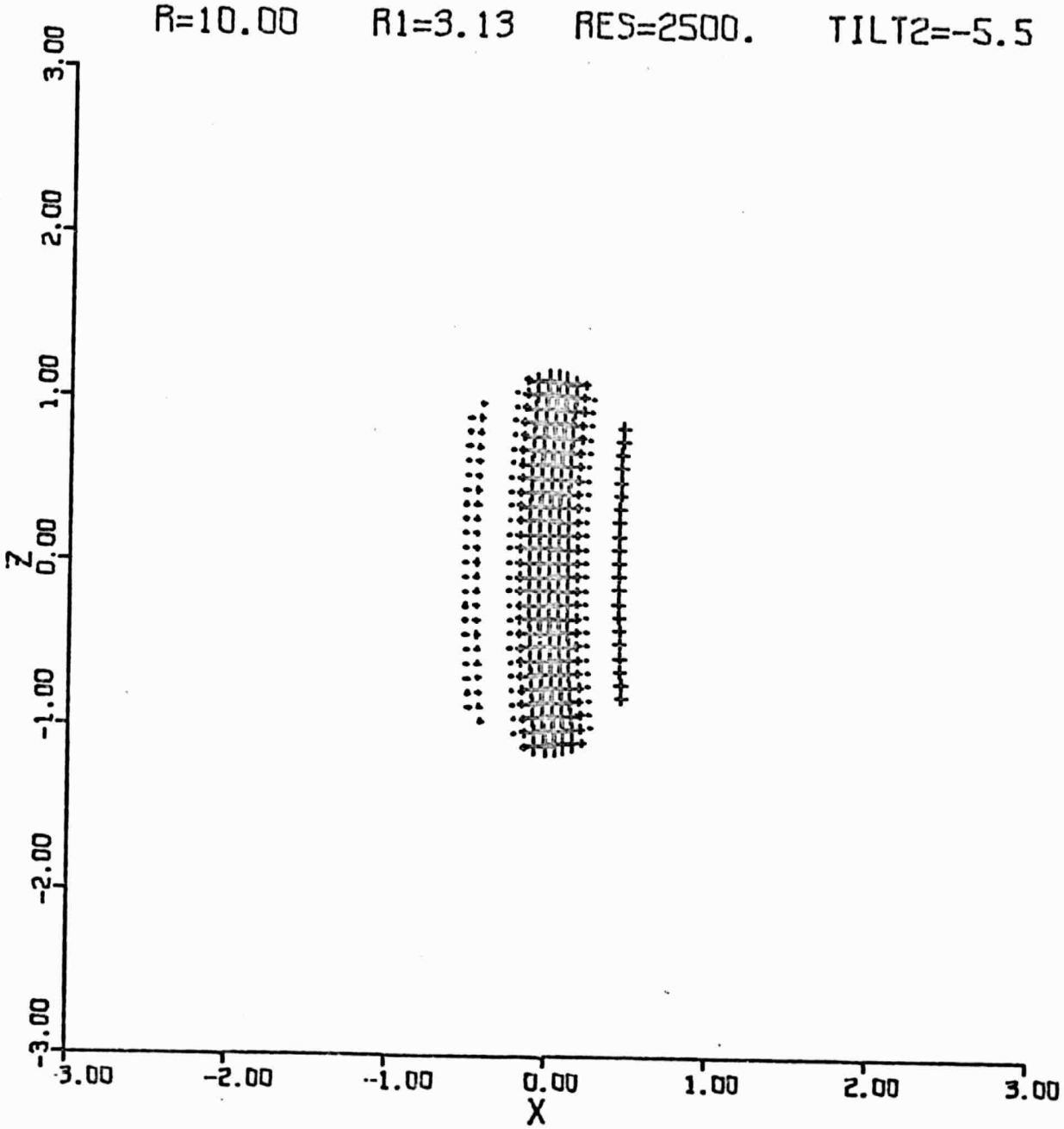

Fig 25

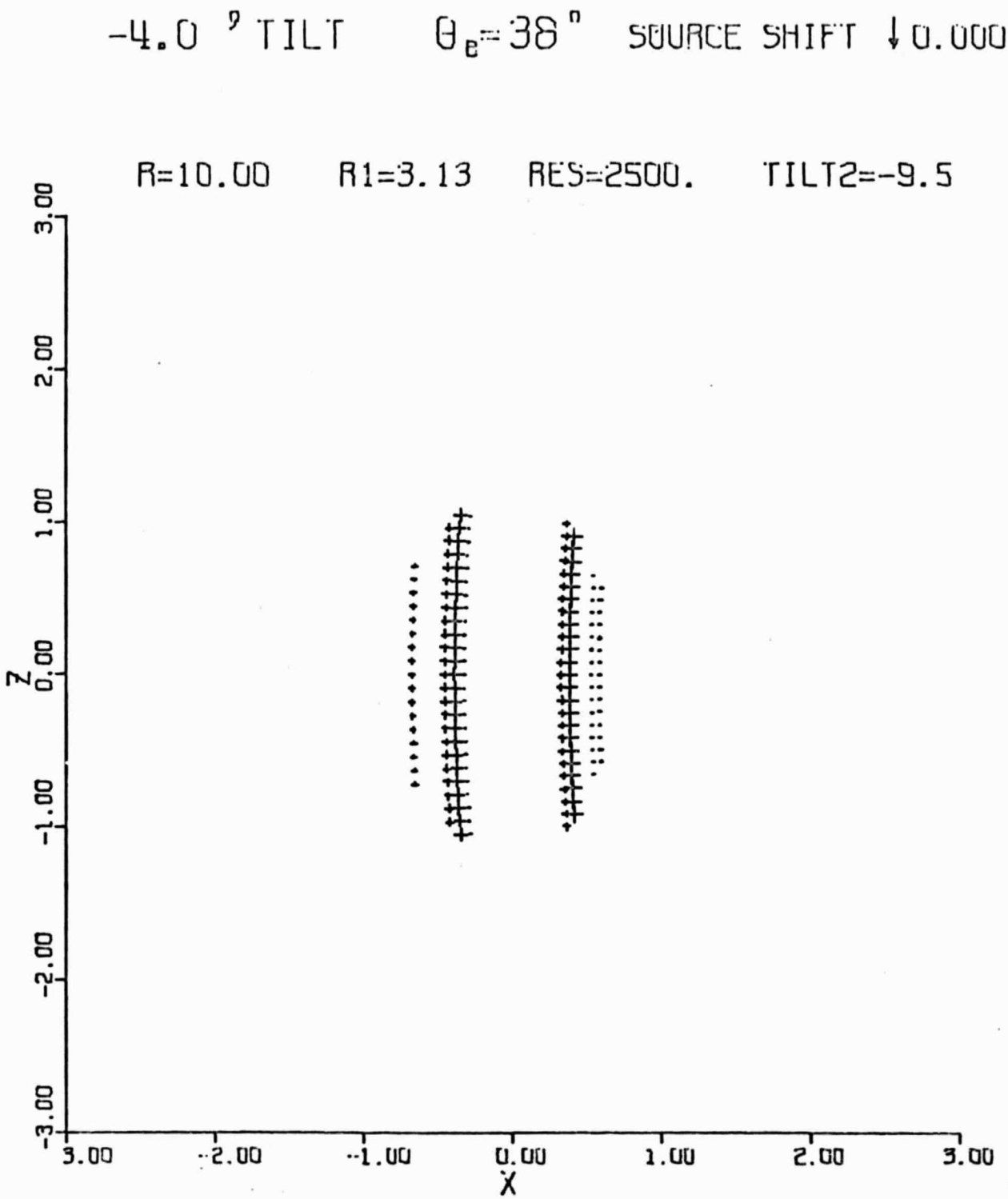
-4.0 ° TILT
θe=38°
SOURCE SHIFT ↓0.000 "
R=10.00
R1=3.13
RES=2500.
TILT2=-9.5
3.00
2.00
1.00
0.00
-1.00
-2.00
-3.00
Z
3.00
2.00
1.00
0.00
-1.00
-2.00
-3.00
X

Fig 26

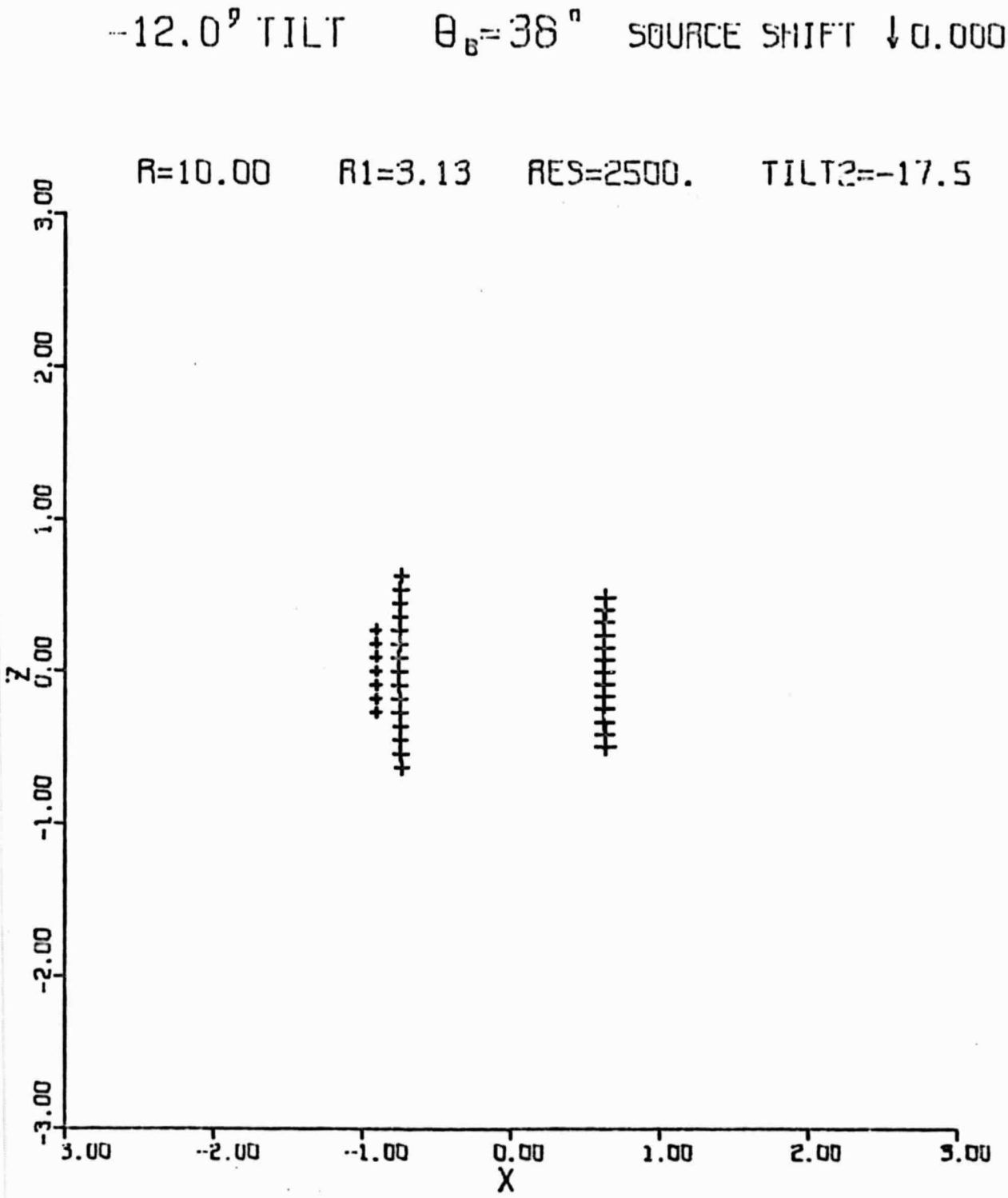
-12.0° TILT θB=38° SOURCE SHIFT ↓0.000 "
R=10.00 R1=3.13 RES=2500. TILT2=-17.5
3.00
2.00
1.00
0.00
-1.00
-2.00
-3.00
Z
-3.00
-2.00
-1.00
0.00
1.00
2.00
3.00
X

Fig 27

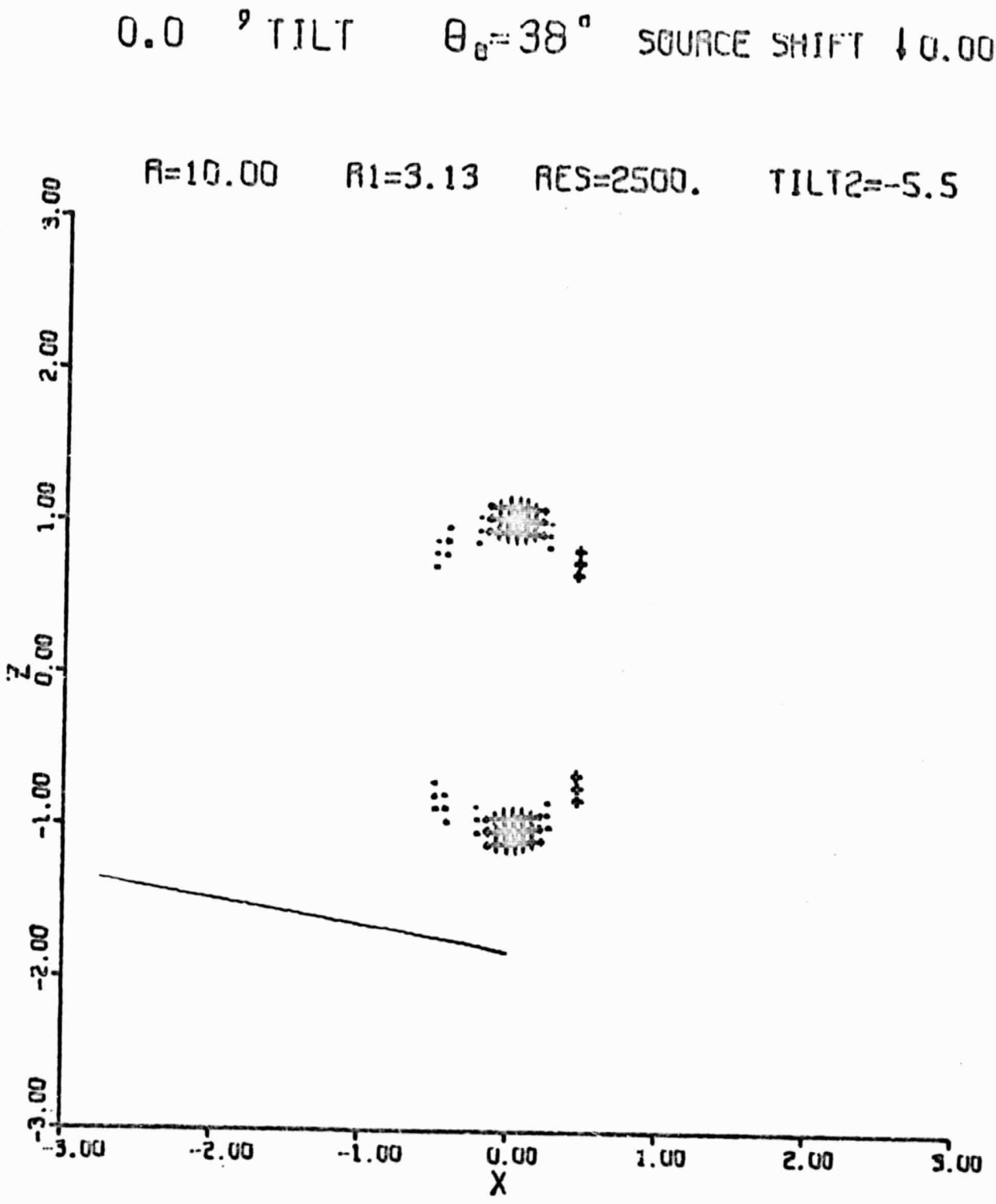
0.0 ° TILT θ₀=38° SOURCE SHIFT ↓0.000
A=10.00 R1=3.13 RES=2500. TILT2=-5.5
3.00
2.00
1.00
0.00
-1.00
-2.00
-3.00
Z
-3.00
-2.00
-1.00
0.00
1.00
2.00
3.00
X

Fig 28

-4.0 ° TILT $\theta_B = 38^\circ$ SOURCE SHIFT ↓ 0.000 "

R=10.00 R1=3.13 RES=2500. TILT2=-9.5

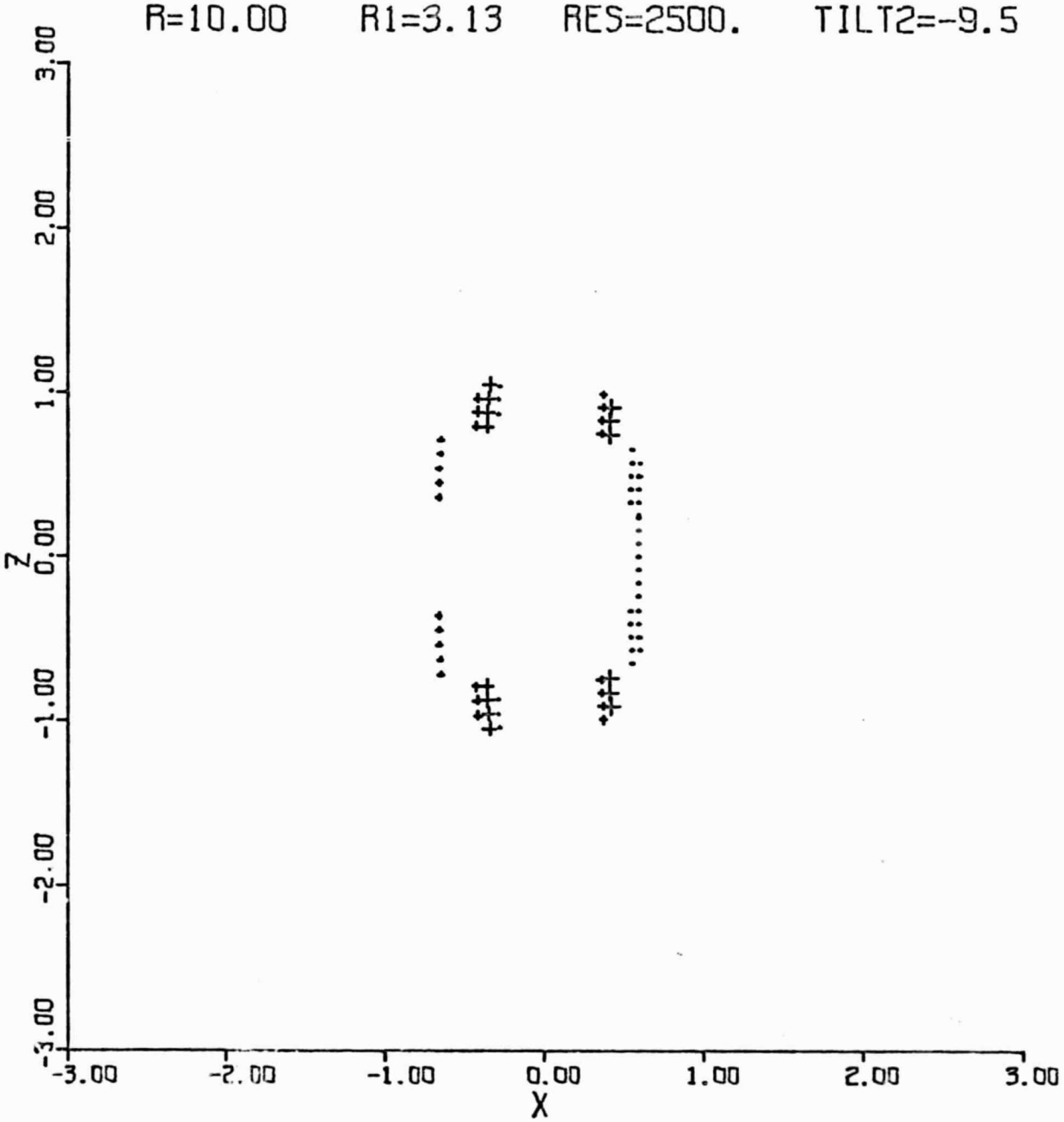

Fig 29

-12.0° TILT θ_B=38° SOURCE SHIFT ↓0.000 "

R=10.00 R1=3.13 RES=2500. TILT2=-17.5

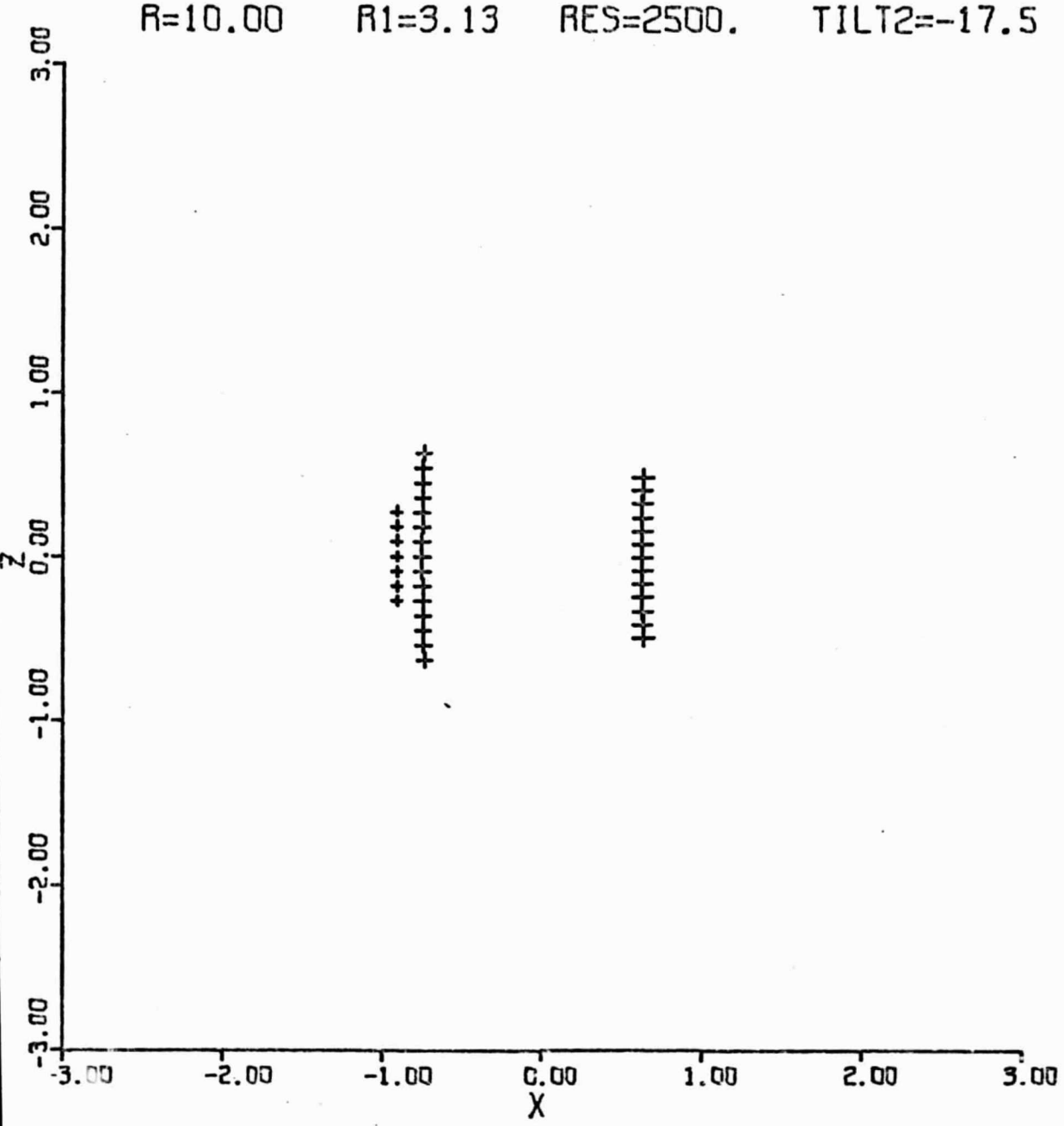

Fig 30

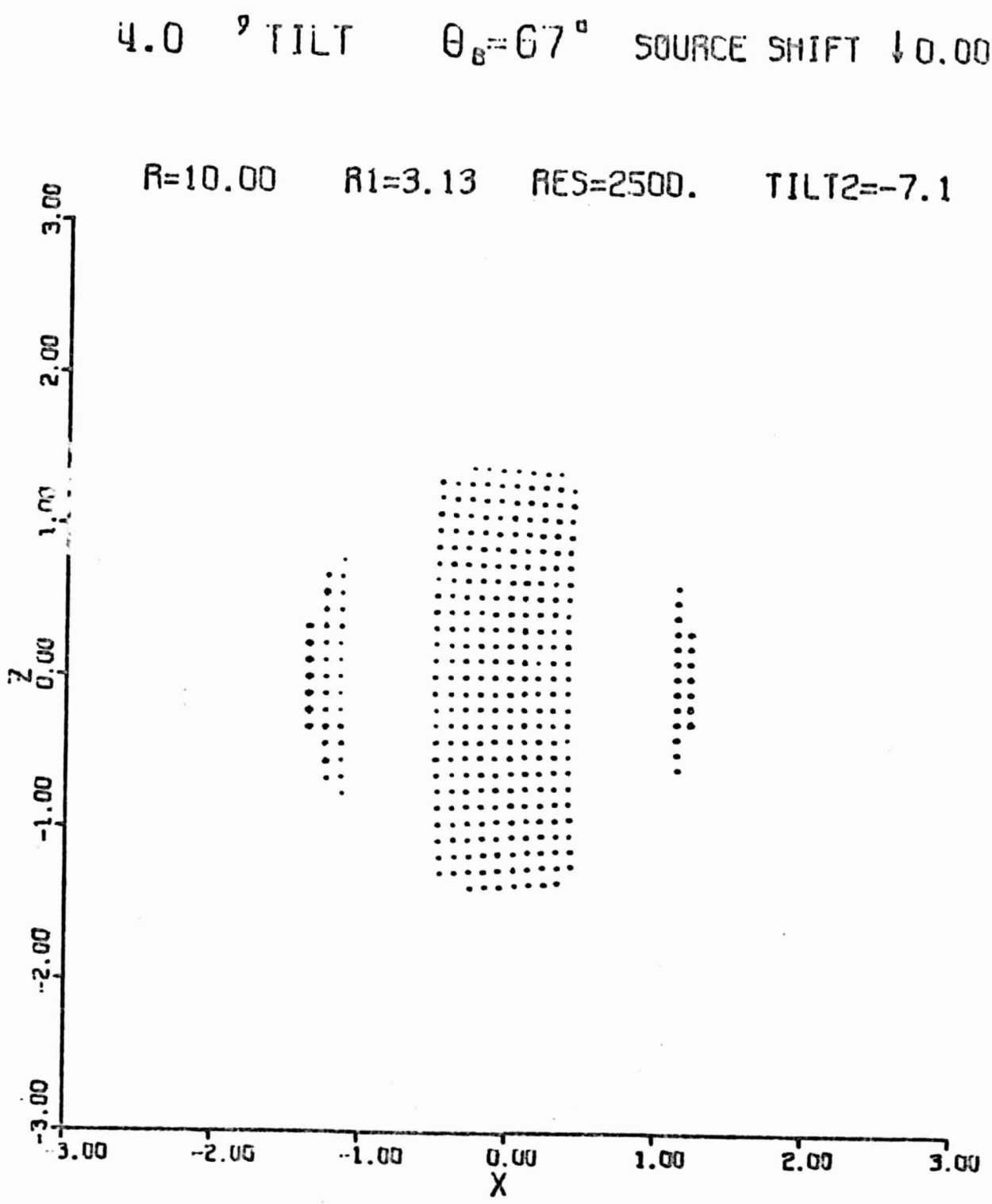
4.0 ° TILT θB=67° SOURCE SHIFT ↓0.000 "
R=10.00 R1=3.13 RES=2500. TILT2=-7.1
3.00
2.00
1.00
0.00
-1.00
-2.00
-3.00
Z
-3.00
-2.00
-1.00
0.00
1.00
2.00
3.00
X

Fig 31

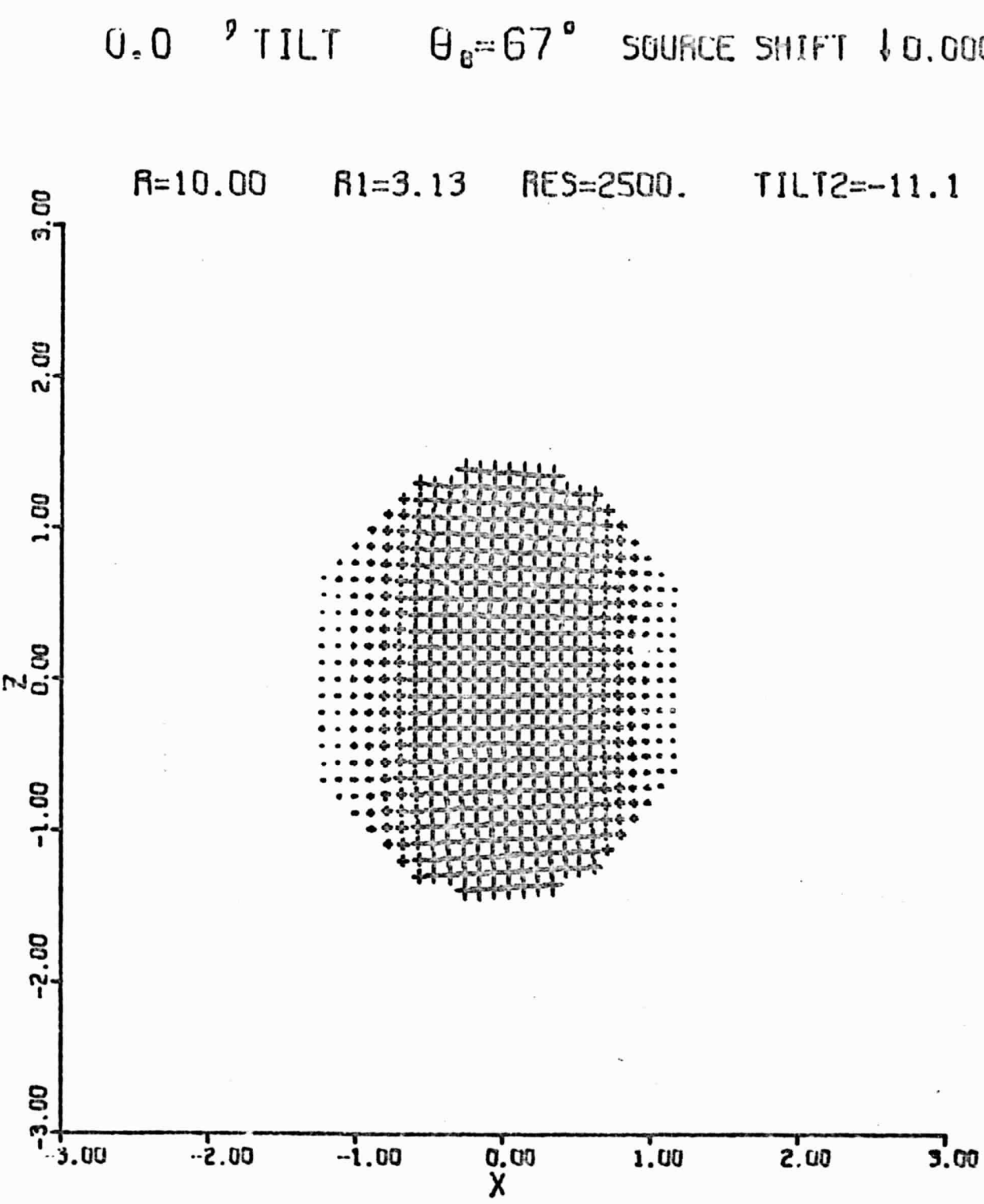
0.0 ' TILT θ_B=67° SOURCE SHIFT ↓0.000 "
R=10.00 R1=3.13 RES=2500. TILT2=-11.1
3.00
2.00
1.00
0.00
-1.00
-2.00
-3.00
Z
-3.00
-2.00
-1.00
0.00
1.00
2.00
3.00
X

Fig 32

-4.0 ° TILT $\theta_B = 67°$ SOURCE SHIFT ↓ 0.000 "

R=10.00 R1=3.13 RES=2500. TILT2=-15.1

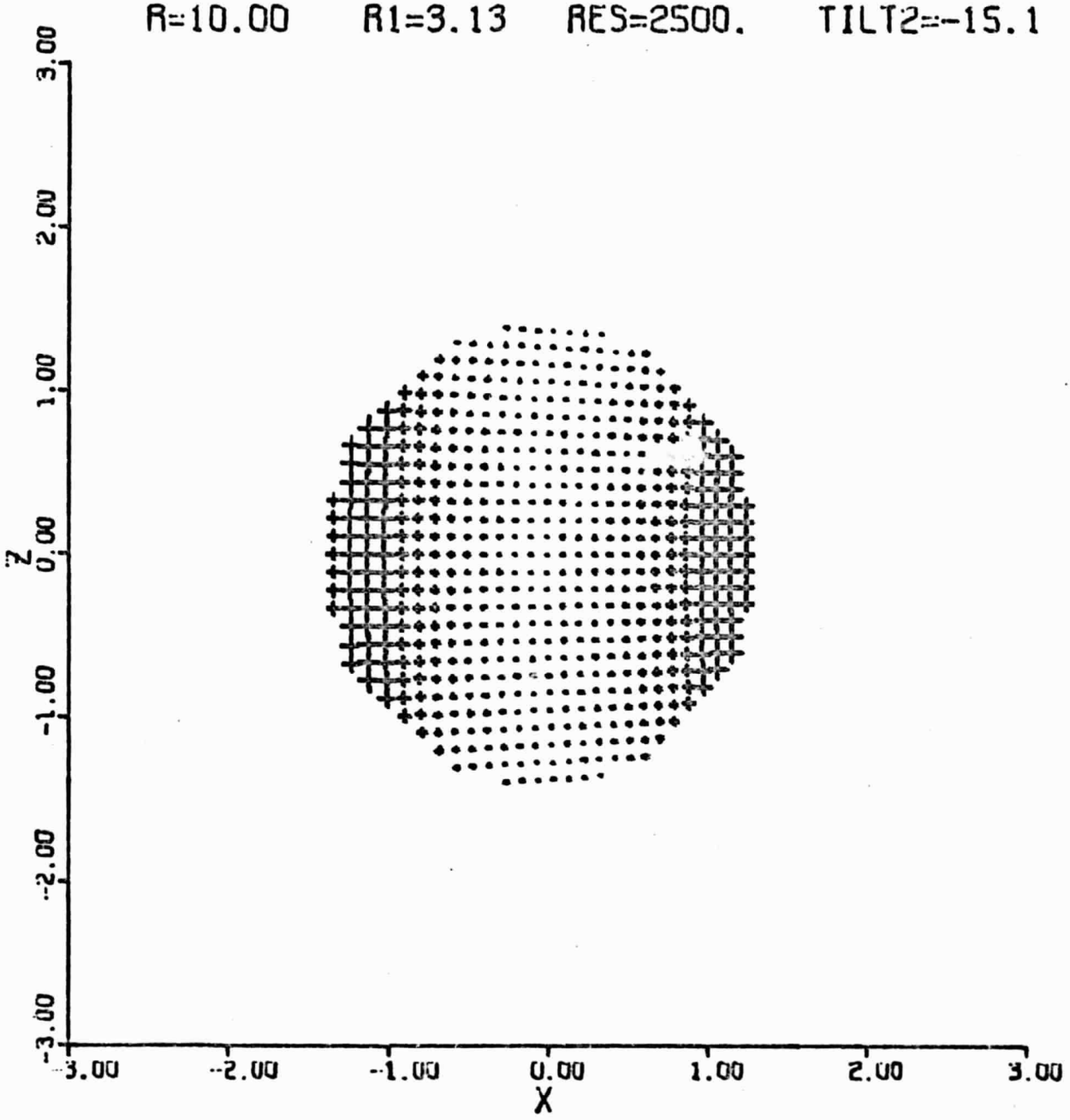

Fig 33

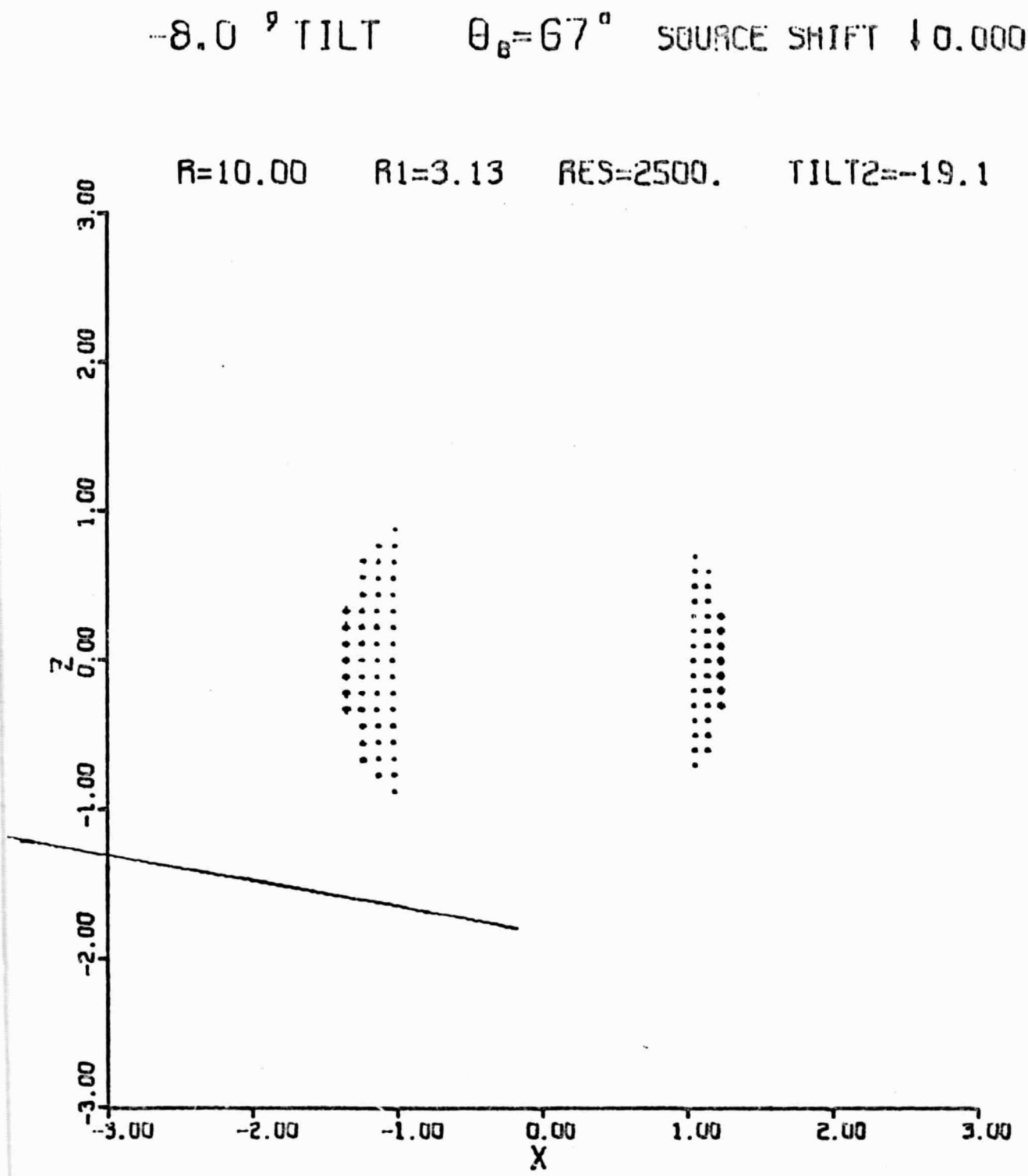
-8.0 ° TILT
θB=67°
SOURCE SHIFT 0.000
R=10.00
R1=3.13
RES=2500.
TILT2=-19.1
3.00
2.00
1.00
0.00
-1.00
-2.00
-3.00
Z
-3.00
-2.00
-1.00
0.00
1.00
2.00
3.00
X

Fig 34

4.0 ° TILT $\theta_B = 67°$ SOURCE SHIFT ↓ 0.000 "

R=10.00 R1=3.13 RES=2500. TILT2=-7.1

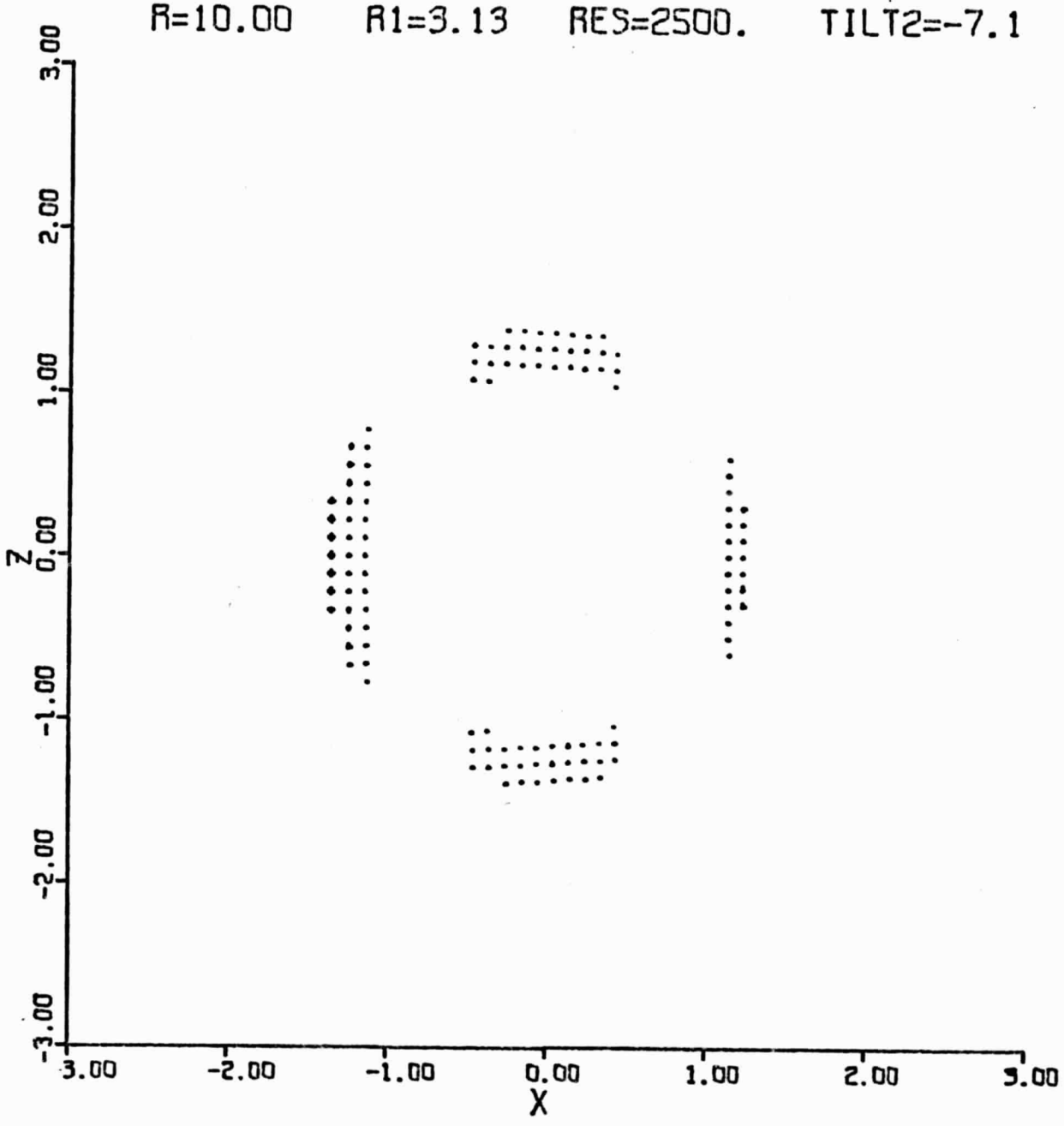

Fig 35

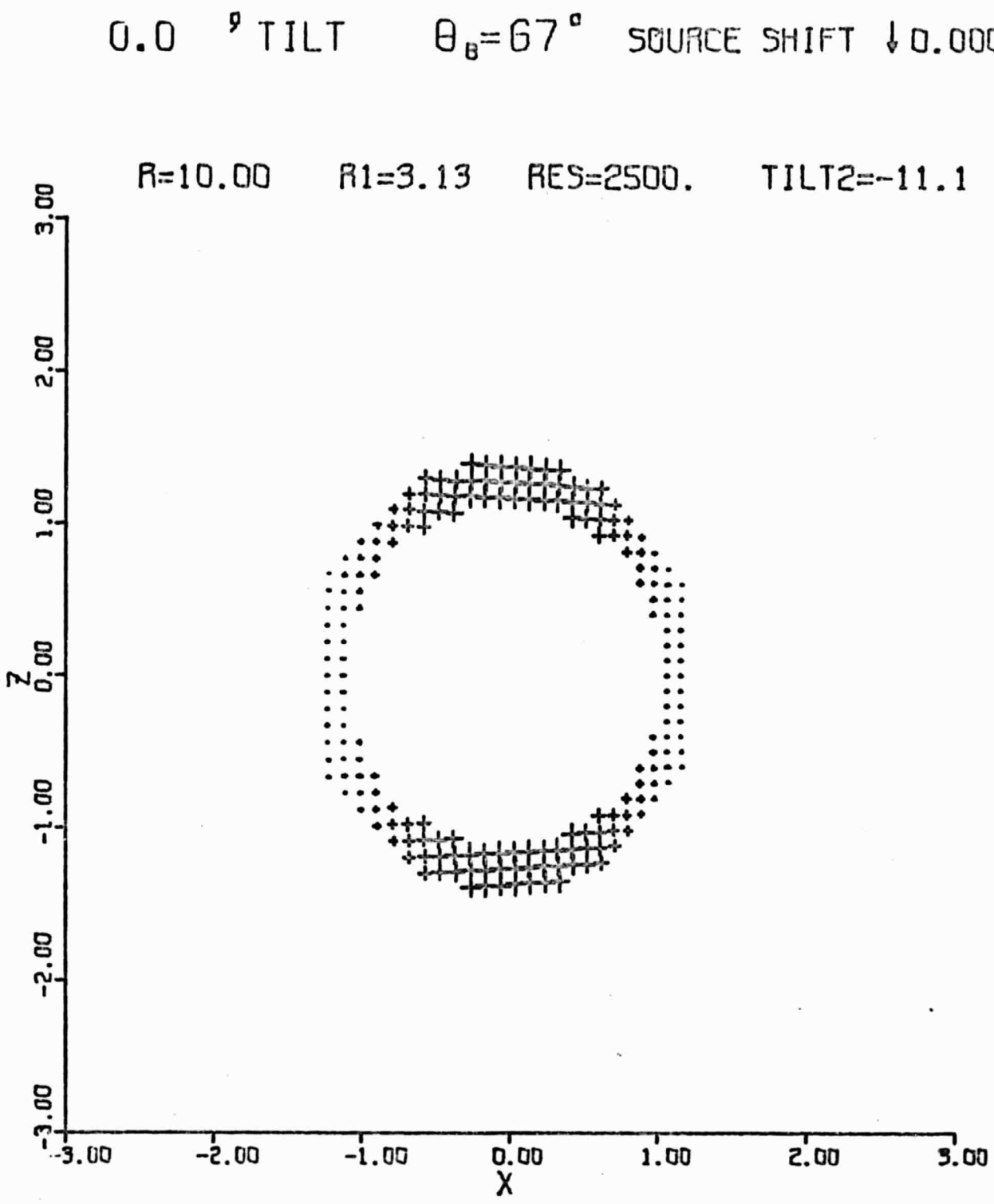
0.0 ° TILT θB=67° SOURCE SHIFT ↓0.000 "
R=10.00 R1=3.13 RES=2500. TILT2=-11.1
3.00
2.00
1.00
0.00
-1.00
-2.00
-3.00
Z
-3.00
-2.00
-1.00
0.00
1.00
2.00
3.00
X

Fig 36

-4.0 ' TILT $\theta_B = 67^\circ$ SOURCE SHIFT ↓ 0.000 "

R=10.00 R1=3.13 RES=2500. TILT2=-15.1

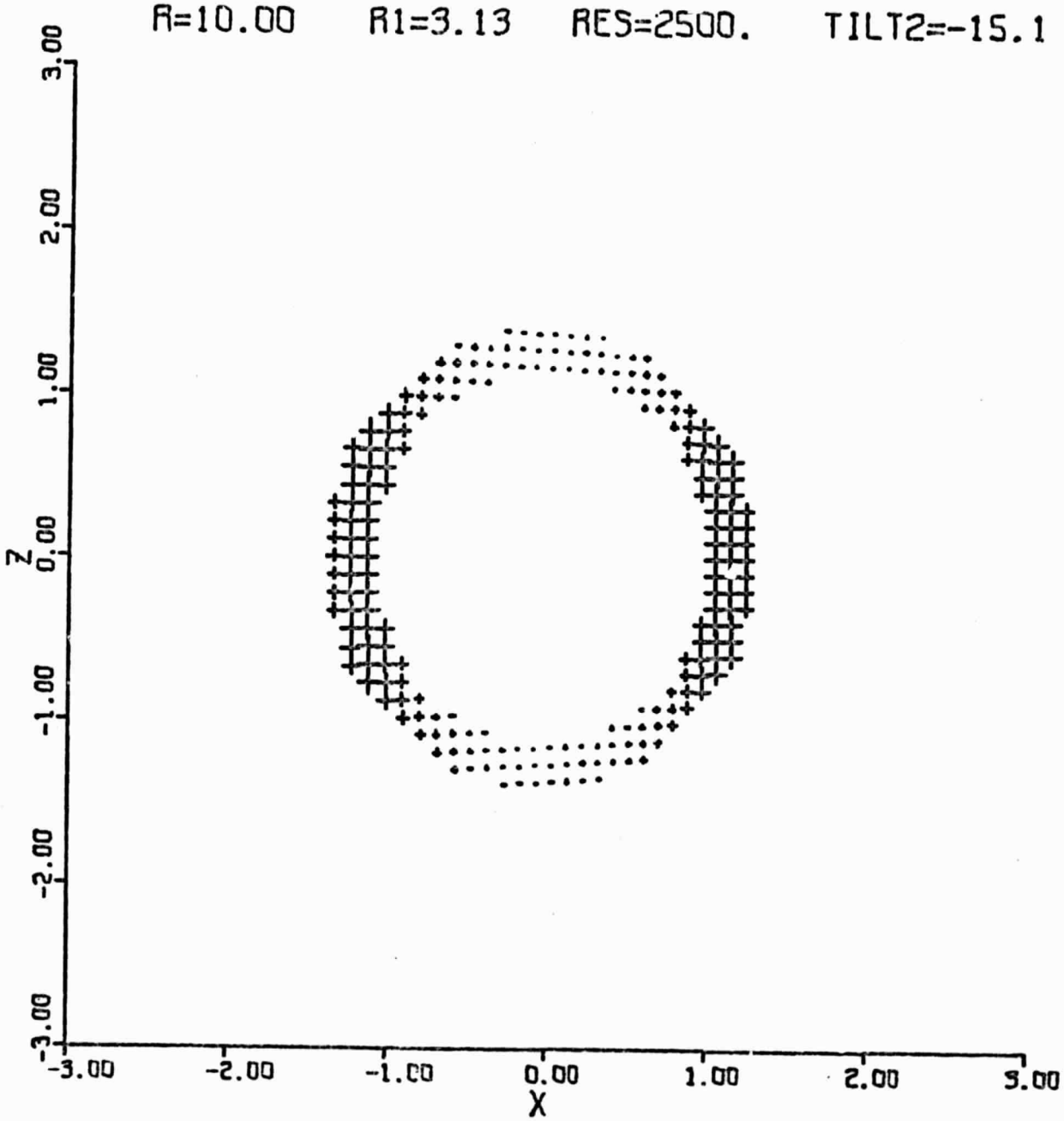

Fig 37

-8.0 ° TILT θ_0=67° SOURCE SHIFT ↓0.000 "

R=10.00 R1=3.13 RE3=2500. TILT2=-19.1

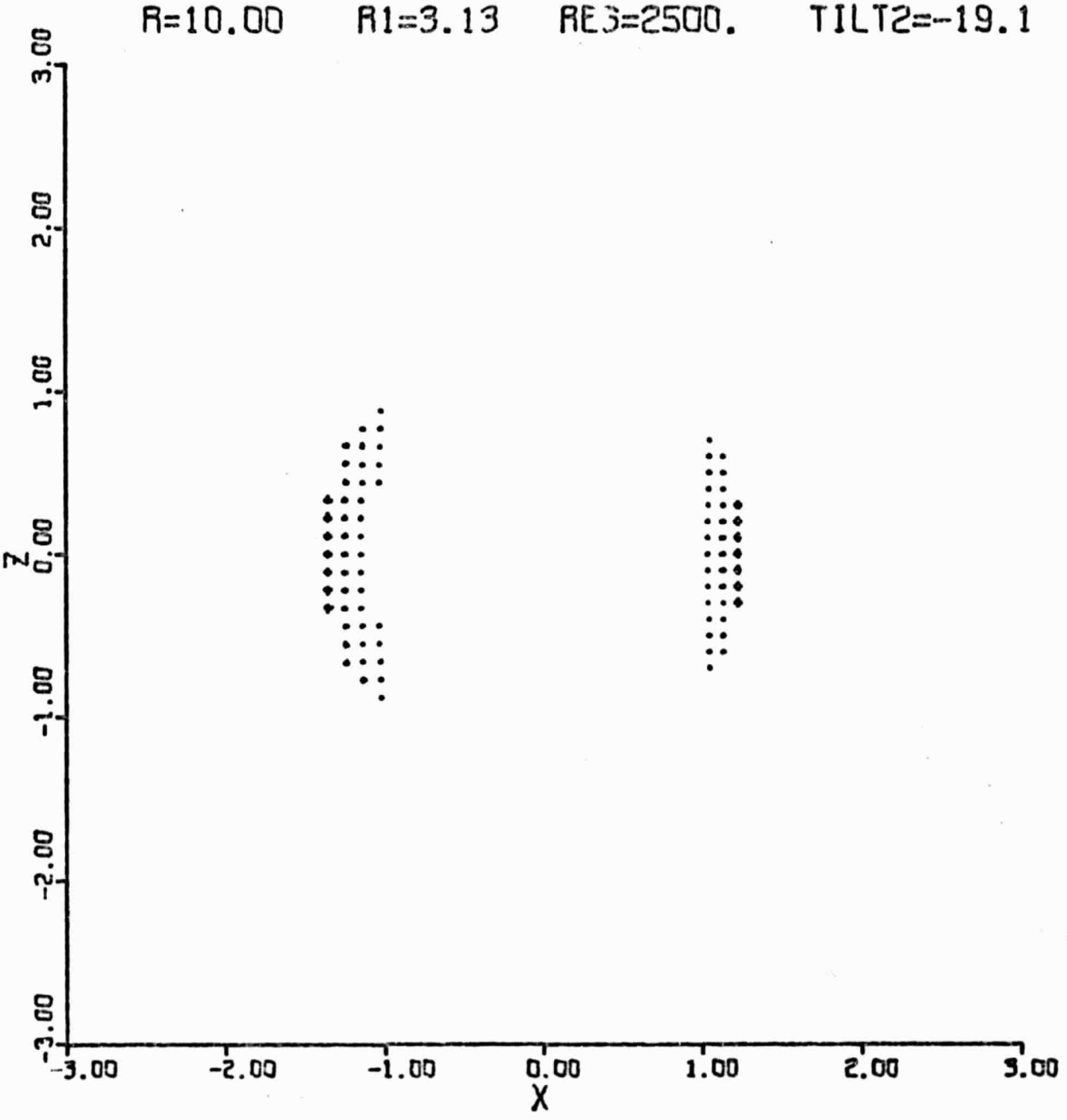

Fig 38

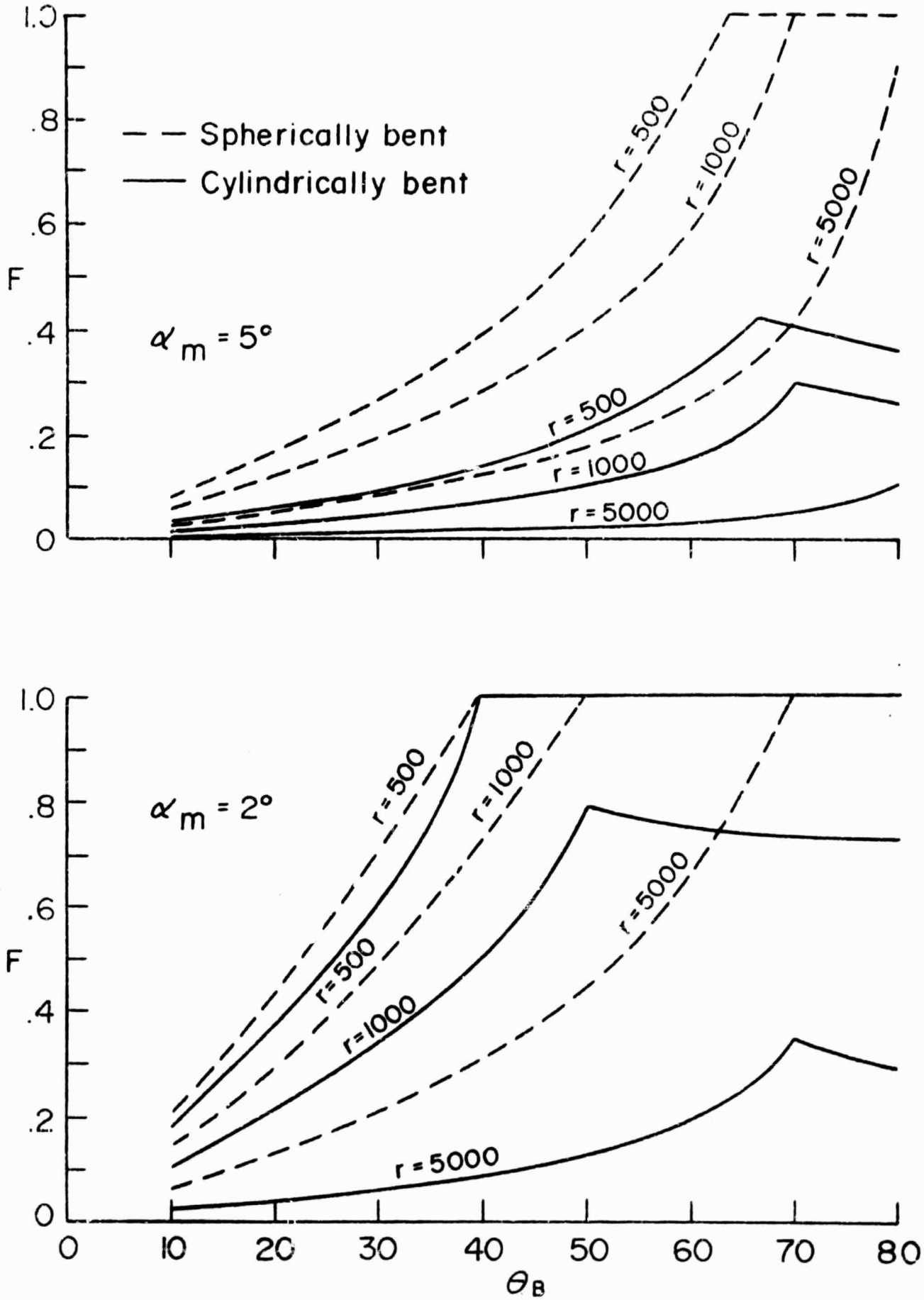
1.0
.8
.6
.4
.2
0
F
— — Spherically bent
—— Cylindrically bent
$\alpha_m = 5°$
r = 500
r = 1000
r = 5000
r = 500
r = 1000
r = 5000
$\alpha_m = 2°$
r = 500
r = 1000
r = 5000
r = 500
r = 1000
r = 5000
0
10
20
30
40
50
60
70
80
θ_B

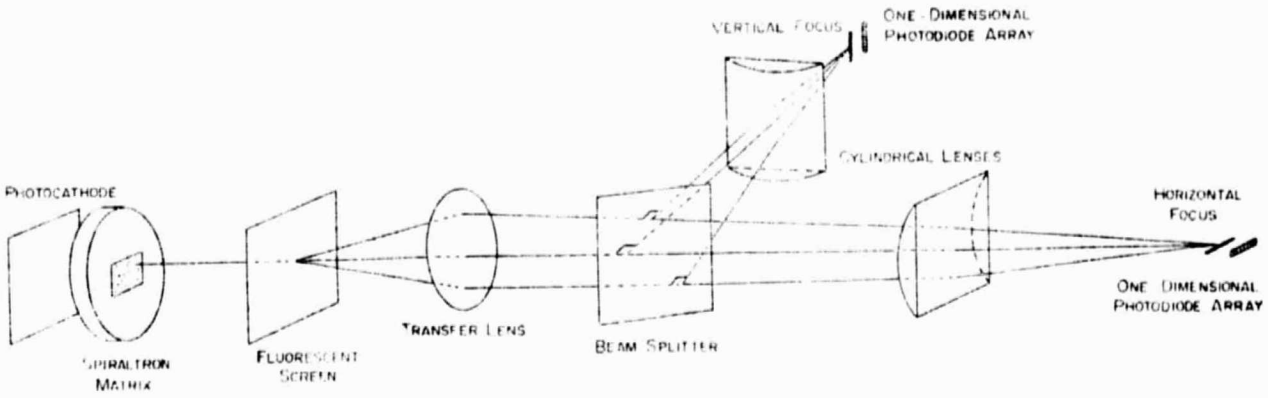

Fig. 40

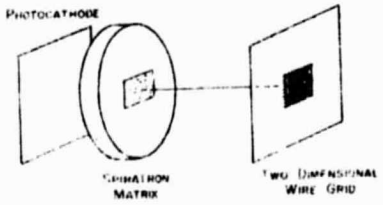

Fig. 41

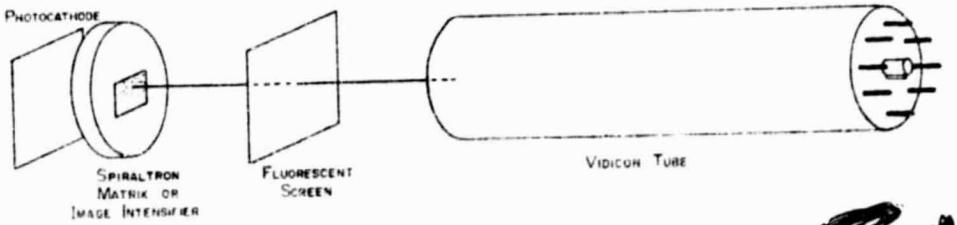

Fig. 42

END